AD-A189 385 A FUNDAMENTAL UNDERSTANDING OF THE EFFECT OF ALLOYING ELEMENTS ON THE COR (U) JOHNS HOPKINS UNIV BALTIMORE MD J KRUGER ET AL 16 NOV 87 AFOSR-TR-87-1892 1/1

UNCLASSIFIED F49620-86-C-0014 F/G 11/6 2 NL

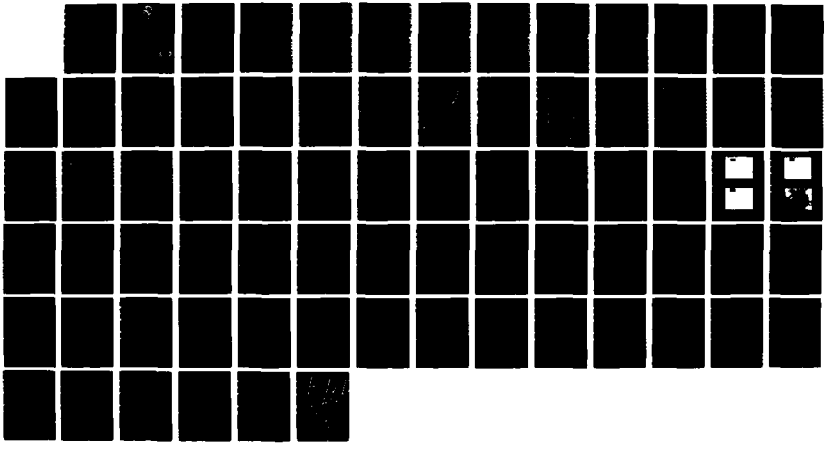

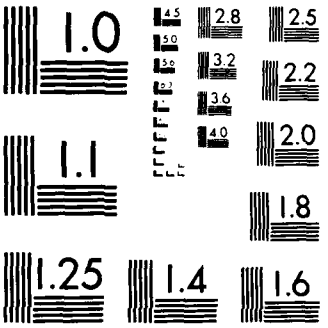

A FUNDAMENTAL UNDERSTANDING OF THE EFFECT OF ALLOYING ELEMENTS ON THE CORROSION RESISTANCE OF RAPIDLY SOLIDIFIED Mg ALLOYS

SECOND ANNUAL REPORT

J. Kruger, G.G. Long, D.K. Tanaka,
A. Joshi and G.L. Makar

November 16, 1987

The Johns Hopkins University

F49620-86-C-0014,P00002
AIR FORCE OFFICE OF SCIENTIFIC RESEARCH

SECURITY CLASSIFICATION OF THIS PAGE

REPORT DOCUMENTATION PAGE

Form Approved OMB No. 0704-0188

1a. REPORT SECURITY CLASSIFICATION: Unclassified	1b. RESTRICTIVE MARKINGS: N.A.
2a. SECURITY CLASSIFICATION AUTHORITY	3. DISTRIBUTION/AVAILABILITY OF REPORT: Unlimited
2b. DECLASSIFICATION/DOWNGRADING SCHEDULE	
4. PERFORMING ORGANIZATION REPORT NUMBER(S): F496620-86-C-0014,P00002	5. MONITORING ORGANIZATION REPORT NUMBER(S): AFOSR-TR- 87-1892
6a. NAME OF PERFORMING ORGANIZATION: Johns Hopkins Univ. / 6b. OFFICE SYMBOL (If applicable):	7a. NAME OF MONITORING ORGANIZATION: Air Force Office Of Scientific Research
6c. ADDRESS (City, State, and ZIP Code): 102 Maryland Hall, Baltimore, MD 21218	7b. ADDRESS (City, State, and ZIP Code): AFOSR, Bldg. 410-NE, Bolling AFB, DC 20332
8a. NAME OF FUNDING/SPONSORING ORGANIZATION: AFOSR / 8b. OFFICE SYMBOL (If applicable): NE	9. PROCUREMENT INSTRUMENT IDENTIFICATION NUMBER: F49620-86-C-0014
8c. ADDRESS (City, State, and ZIP Code): Bldg.410-NE, Bolling AFB, DC 20332	10. SOURCE OF FUNDING NUMBERS: PROGRAM ELEMENT NO. 61102F / PROJECT NO. 2306 / TASK NO A1 / WORK UNIT ACCESSION NO.

11. TITLE (Include Security Classification)
A Fundamental Understanding of the Effect of Alloying Elements on the Corrosion Resistance of Rapidly Solidified MG Alloys

12. PERSONAL AUTHOR(S)
J. Kruger, G.G. Long, D.K. Tanaka, A. Joshi, and G.L. Makar

13a. TYPE OF REPORT	13b. TIME COVERED	14. DATE OF REPORT (Year, Month, Day)	15. PAGE COUNT
Annual	FROM 11-1-86 TO 10-31-87	87-11-16	71

16. SUPPLEMENTARY NOTATION

17. COSATI CODES			18. SUBJECT TERMS (Continue on reverse if necessary and identify by block number)
FIELD	GROUP	SUB-GROUP	Mg alloys, rapidly solidified alloys, corrosion, EXAFS, electrochemistry, localized corrosion, passivity.

19. ABSTRACT (Continue on reverse if necessary and identify by block number)

During the second year of this project progress was made in the following areas concerned with the effect of alloying elements on the corrosion resistance of RSP Mg alloys:

1) The development of the surface reflection x-ray spectroscopic technique (reflEXAFS) to carry out structural studies on the films on Mg alloys that control corrosion was completed and applied in measurements at the oxygen K-edge of surface films on high purity Mg and AZ61 Mg alloys. The existence of magnesium hydroxide on these surfaces was found.
2) Electrochemical studies of the effect of Al, An, Ce, Nd, Y, Mn, Li, and Ca in melt-spun Mg alloy ribbons on corrosion behavior were carried out. The corrosion rate decreased with increased percentages of Al and small additions of Zn. It was found that rapid solidification improves the resistance of the alloy studied (AZ61) to localized Cl^- attack.
3) Surface analytical studies found that only Li and Ca in the RSP Mg alloys have a tendency to be enriched in the films on these allys. Hydroxides and carbonates were also found in the surface films along with oxides.

20. DISTRIBUTION/AVAILABILITY OF ABSTRACT	21. ABSTRACT SECURITY CLASSIFICATION
☐ UNCLASSIFIED/UNLIMITED ☐ SAME AS RPT ☐ DTIC USERS	Unclassified
22a. NAME OF RESPONSIBLE INDIVIDUAL: ~~J. Kruger~~ Rosenstein	22b. TELEPHONE (Include Area Code): ~~(301) 338-~~ 6933 / 22c. OFFICE SYMBOL: NE

DD Form 1473, JUN 86 — Previous editions are obsolete. — SECURITY CLASSIFICATION OF THIS PAGE

A FUNDAMENTAL UNDERSTANDING OF THE EFFECT OF ALLOYING ELEMENTS ON THE CORROSION RESISTANCE OF RAPIDLY SOLIDIFIED Mg ALLOYS

J. Kruger, G.G. Long, D.K. Tanaka,
A. Joshi and G.L. Makar

ABSTRACT

During the second year of this project progress was made in the following areas concerned with the effect of alloying elements on the corrosion resistance of RSP Mg alloys:

1) The development of the surface reflection x-ray spectroscopic technique (reflEXAFS) to carry out structural studies on the films on Mg alloys that control corrosion was completed and applied in measurements at the oxygen K-edge of surface films on high purity Mg and AZ61 Mg alloy. The existence of magnesium hydroxide on these surfaces was found.

2) Electrochemical studies of the effect of Al, Zn, Ce, Nd, Y, Mn, Li, and Ca in melt-spun Mg alloy ribbons on corrosion behavior were carried out. The corrosion rate decreased with increased percentages of Al and small additions of Zn. It was found that rapid solidification improves the resistance of the alloy studied (AZ61) to localized Cl^- attack.

3) Surface analytical studies found that only Li and Ca in the RSP Mg alloys have a tendency to be enriched in the films on these alloys. Hydroxides and carbonates were also found in the surface films along with oxides.

INTRODUCTION

This Second Annual Report describes the progress achieved in the past year in three parts:

PART I-- The EXAFS studies of the structure of films on Mg alloy surfaces that control corrosion resistance are described in this section. The development of the reflEXAFS technique (especially the data analysis aspects) that enables the structure and composition of films on bulk alloy surfaces to be determined that was initiated in the first year has been completed. Results have been obtained on the films on pure Mg and a Mg alloy (AZ61). It was still not possible to examine the films on RSP Mg ribbons but an extruded alloy produced from rapidly solidified particulates was graciously provided by Drs. Chang and Das of Allied Signal Corp. which will now make it possible to carry out reflEXAFS measurements on films on RSP Mg surfaces. Such measurements will be made in November and December 1987 at the National Synchrotron Light Source at Brookhaven.

PART II-- This is a continuation of the studies initiated in the first year to evaluate the role of alloying elements on corrosion behavior using electrochemical and gravimetric techniques. The effect of the alloying elements Al, Zn, Ce, Nd, Y, Mn, Li, and Ca on the corrosion rates of melt-spun ribbons supplied by Lockheed was examined. The corrosion rates of the extruded alloys from Allied Signal Corp. mentioned above were also measured.

PART III-- This is the report submitted by Lockheed, a sub-contractor for the first and second years of this contract, detailing surface analytical studies of the films on RSP Mg alloys and additional corrosion data. They have requested a no cost extension to enable them to carry out further studies during the third year.

PART I--To be submitted, revised and expanded, to J. of Electrochem. Soc.

Structure of Surface Films on Magnesium and Magnesium Alloys

G.G. Long
National Bureau of Standards
Gaithersburg, MD 20877
and
J. Kruger, D.K. Tanaka, and Z. Zhang
The Johns Hopkins University
Baltimore, MD 21218

In recent years, there has been considerable interest in the possible use of magnesium alloys for aerospace applications because of the substantial weight savings that would result. The poor corrosion resistance of these alloys, which has been a major barrier to their application in the past, is now being addressed through methods such as rapid solidification which have recently been shown to produce materials with significantly improved corrosion resistance and mechanical strength [1].

The improved corrosion resistance is expected to be mainly due to the creation of an improved passive film on the surface of these alloys. The corrosion protection of magnesium and its alloys is related to the formation of magnesium-oxide and magnesium-hydroxide in surface films on the material, and to the stability of these films in various environments.

This study was undertaken to determine the role of alloying elements on the nature (structure, composition, and electronic properties) of the films that form on pure

magnesium and magnesium alloys, with the goal being to gain an understanding of the factors that promote the formation of improved passive films through modern processing techniques.

About 10 years ago, Revesz and Kruger[2] suggested that a noncrystalline structure is generally more desirable for a successful passive film than a crystalline structure. Of the many available (x-ray, neutron and electron) scattering techniques, only x-ray absorption spectroscopy offers a direct surface-sensitive measurement of the (possibly) disordered structure of passive films on alloys. The challenge in such measurements is to study the passive film, which is often only of the order of a few nm thick, on the surface of a bulk metal or alloy containing many of the same elemental species. Two EXAFS techniques are available for such surface sensitive measurements. One is to employ partial yield electron detection, either in vacuum[3] or in the inert atmosphere of a photocathode detector[4], and the other is to follow the x-ray absorption through the use of surface reflectance measurements[5]. The latter technique is particularly suited for measurements on ultra-thin layers of oxide on low-Z alloys because of the excellent signal-to-noise that accompanies the surface sensitivity at moderate reflection angles. The results reported in this work were derived from surface reflectance measurements of the thin films on magnesium and magnesium alloys in the neighborhood of the oxygen K-edge.

ENERGY-DEPENDENT REFLECTANCE

The high reflectivity of x-rays at grazing incidence to a polished surface can be described using the Fresnel equations. These equations are derived from a consideration of plane waves incident on a planar boundary. Several conditions must be met for these assumptions to be valid: 1. the radius of curvature of the surface must be much greater than the wavelength of the light; 2. the reflecting medium is assumed to be homogeneous; and 3. the reflecting surface is assumed to be planar. The first condition is easily satisfied for x-rays. With regard to the second condition, even though the magnitude of the x-ray wavelengths is of the same order as the atoms, there is no experimental evidence that the reflecting medium does not behave as if it were homogeneous[6]. Because of the small surface area involved, pits and scratches in the surface detract little from the expected reflectivity. Microscopic roughness, however, can have serious reflectivity, and this will be discussed further below.

The complex dielectric permeability is given by

$$\kappa = 1 - 2\delta - 2\beta i \qquad (1)$$

The dielectric permeability determines the phase velocity of waves in the medium

$$v = c/\sqrt{\kappa} ,$$

and the complex refractive index is n = . If both and are much less than 1, then to first order

$$n = 1 - \delta - \beta i \qquad (2)$$

In this approximation, $1-\delta$ is related to the real part of the phase velocity of the wave in the medium and β is related to the absorption that we wish to measure. δ, which is called the unit decrement, is of the order of 10^{-5}-10^{-6} for hard ($\sim$0.1 nm) x-rays, but is closer to 10^{-2}-10^{-3} for the softer ($\sim$2.5 nm) relevant to this work. This means that second order corrections involving δ may be significant in soft-x-ray measurements. Generally, δ is always positive, so the refractive index for x-rays is less than 1. For a particular group of x-rays, the contribution to δ may be negative, as for wavelengths close to an absorption edge. Usually, however, the contributions to δ from other groups of electrons are positive so that the overall δ is still positive.

The critical angle for total reflection is defined in terms of δ as $\phi_c = \sqrt{2\delta}$. Although the reflectance is not actually equal to 1 at angles smaller than this, it can be quite high for reflectors that have negligible absorption. The behavior of the reflectance as a function of normalized glancing angle is shown for values of β/δ between zero and 1 in Fig. 1. For small values of β/δ, the value of the critical angle is defined. If the inflection point of the reflectance curve is chosen for the value of the critical angle, then we note that for β/δ larger than 0.63 the reflectance curves do not display an inflection point. The

reflectance, however, is still accurately predicted by the theory.

The ratio for the amplitude of the reflectance is given by

$$\text{Amplitude} = E_{\perp}/E_{0\perp} \qquad (3)$$

where $\perp$ indicates that the electric vector is perpendicular to the plane of incidence. If we set $\phi = a + bi$, then the reflectance we measure can be written

$$R = \frac{(\phi - a)^2 + b^2}{(\phi + a)^2 + b^2}$$

where

$$a^2 = \tfrac{1}{2}\left[\sqrt{(\phi^2 - 2\delta)^2 + 4\beta^2} + (\phi^2 - 2\delta)\right],$$

$$b^2 = \tfrac{1}{2}\left[\sqrt{(\phi^2 - 2\delta)^2 + 4\beta^2} - (\phi^2 - 2\delta)\right].$$

For the present study, the values of δ and β, both of which carry EXAFS information, are calculated for magnesium-oxide using equations that are valid close to the K-edge of oxygen[7,8].

Under "total" reflection conditions, there is no wave propagating into the medium. Instead, there are waves of varying amplitude (evanescent waves) present which decrease with increasing penetration. These waves enter the medium and then emerge again from the same surface. The 1/e penetration depth, d, can be calculated from the imaginary part of the reflectance (b) using

$$d = \lambda/4\pi b$$

where λ is the wavelength of the radiation.

Fig. 2 shows the penetration depth in MgO as a function of angle for a range of energies relevant to studies near the oxygen K-edge, where, for the purposes of calculation, the effects on δ are assumed to be dominated by oxygen is

electrons. For angles less than approximately 2.3°, the penetration depth for all photon energies up to 800 eV is less than 3.0 nm.

Outside the region for "total" reflection, interference can take place for a thin film on the surface of a substrate. The periodicity of the interference pattern can be used to measure the thickness of such films if they are uniform.

Since the wavelengths of x-rays are about 1000 times smaller than those of visible light, there is an increased concern about the smoothness of the reflecting surface. Since the glancing angle for x-rays is about 100 times smaller than for optical, the quality of the reflecting surface should be of the order of 20 times better.

EXPERIMENTAL

The corrosion protection of magnesium and its alloys is related to the formation of magnesium-oxide and magnesium-hydroxide in surface films on the material, and the stability of these films in various environments. EXAFS measurements on these films presents a considerable challenge, not the least of which is the positions of the K-edges of Mg and O, which are at 1303 and 543 respectively. Both of these edges are in the soft x-ray range of the electromagnetic spectrum. Photons around the former energy are available at only a few x-ray synchrotron beam-stations in the world. Photons in the oxygen K-edge range are more

readily available, but there are problems with the properties of detectors and the sample environment. Just as the photocathode proportional counter enabled the surface-sensitive hard x-ray EXAFS measurement of thin films on bulk substrates, here it is required to measure the EXAFS of the surface film on bulk Mg and Mg-alloys using soft x-rays. This suggests a soft x-ray refl-EXAFS measurement at the oxygen K-edge for these materials.

Samples of pure magnesium, AZ61 magnesium alloy, and single crystal MgO standard were polished to a mirror-like finish. Thin films were grown on the metal and the alloy by heating in an oven at 100 C in a humid atmosphere.

The surface reflectance measurements were performed on the U-15 beamline (SUNY/NSLS) at the National Synchrotron Light Source at Brookhaven National Laboratory. The beamline is equipped with a toroidal grating monochromator (TGM) with a 600 line/mm gold coated grating. The TGM has a constant wavelength resolution which depends on the size of the aperture in front of the grating and on the electron beam in the storage ring. A gold mirror is used to direct the monochromated beam toward the experimental station. There is a non-negligible amount of harmonic contamination up to photon energies of 700 eV. The relative intensity of second order in the 480-700 eV part of the spectrum was provided[9,7] using a variable absorber technique. The beamline also has a 150 nm aluminum contamination barrier which separates the sample area from the storage ring

vacuum. This barrier enables soft x-ray absorption measurements under flexible environmental conditions, but it also contributes a flux jump of a few percent at the oxygen K-edge due to the oxide layer on the aluminum. A slight kink at 850 eV is due to Wood's anomaly[10]. For most oxides, the kink appears as a glitch in the EXAFS spectra around 9Å^{-1} in k-space. Since it is not clear as yet what the best correction for this is, all of the spectra are truncated before this feature.

The geometry of the reflEXAFS experiment is shown in Fig. 3. THe soft x-rays entering the sample area impinge first on a (85% transparent) gold mesh coated with P31 phosphor [11] for the beam monitor, I_o, measurement. The remainder of the beam impinges at grazing ($0.5° < \phi < 3.5°$) incidence on the sample and the reflected beam is measured. Both photomultiplier detectors measure soft x-rays via the same x-ray-to-visible conversion phosphor. Although the sample is centered in the beam, a small amount of the unreflected beam passes above the sample and serves to permit a direct measurement of the reflection angle from the position of the reflected beam, I, detector. During the reflEXAFS measurements, a beamstop prevents the unreflected beam from reaching the I detector.

The first part of the data treatment is to remove instrumental factors from the raw data. The spectral range for the measurements is from 480-1000 eV. A measure of the window transmission function over this spectral range is

provided by scans performed without the sample in the beam. Next, separate corrections for harmonic content in I and I_o must be made. These separate corrections are required because part of the second order flux is removed by the reflection process. The I_o correction is carried out straightforwardly using the data from refs. 9 and 11. An estimate of the reflectivity in second order is provided by assuming that a measure of the reflectivity in the range E = 700 - 800 eV, where second order is negligible in the incident beam, approximates the second order reflectivity at E/2 = 350 - 400 eV. Then a measure of the second order contribution to the 480 -700 eV range is provided by the reflectivity data and its extrapolation to the 960 - 1400 eV range. Finally, the reflected intensity I is divided by the incident beam intensity I_o to remove the fluctuations in the incident beam intensity.

After these corrections, the contribution due to electrons other than oxygen K is fitted using a Victoreen* function and the EXAFS function is determined through the fitting and subtraction of a cubic spline. Part of the set of corrected reflectivity spectra for the single crystal MgO standard is shown in Fig. 4.

*The Victoreen function is $Ax^3 + Bx^4$, where A and B are constants and x is the variable under consideration.

RESULTS

For each sample, reflEXAFS data was accumulated for at least four, and usually seven, different grazing angles. Rather than invert the data sets to obtain a single spectrum of for each specimen, each scan was individually inverted and the EXAFS functions analyzed. The EXAFS function, using a ϕ of 1.5^{o} , for single crystal MgO and for the thin film on Mg and AZ61 are shown in Figs. 5, 6, and 7. The excellent signal-to-noise in these spectra are evident. The fundamental due to the r_1 coordination shell and the higher frequencies are clearly visible for both these examples, although the higher frequencies are more pronounced in the case of MgO. The magnitude of the Fourier transform that is derived for these data are shown in Figs. 8, 9, and 10. The result for MgO shows very pronounced higher order shells because of the focusing effect that is seen in scattering in the sodium-chloride structure. In this structure, the oxygen atom's fourth neighbor is directly behind the first neighbor, and the seventh is behind the second. By comparison, the $Mg(OH)_2$ structure is hexagonal with one molecule per unit cell.

The fitting parameters listed in Table 1 are derived by producing theoretical curves that exactly fit the experimental curves (Figs. 5, 6, and 7). The parameters that result in the best match between the theoretical and

the experimental curves are the parameters that describe the structure of the films on Mg alloys that control corrosion.

Two shell fits to the first peak in the Fourier transform for these data yield distances, coordination numbers, and values for σ^2, the Debye-Waller factor which is a measure of the degree of disorder. The O - Mg and O - O distances for the standard and for the films were the same within 0.002 nm. This is not surprising since the known bond distances in MgO and $Mg(OH)_2$ are almost identical. The coordination measured for the single crystal is the effective coordination mentioned above. The coordinations measured in the thin films, however, are the usual spherically averaged coordinations. The N's for the films were significantly below those expected for MgO. Finally, the disorder measured in the films was greater than that measured in the crystals.

Taken together, the results indicate that the thin films on Mg and the AZ61 alloy are not pure MgO. The data suggest that the composition may include a significant fraction of $Mg(OH)_2$ or that the film on AZ61 is less ordered than the MgO single crystal.

REFERENCES

1. C.F. Chang, S.K. Das, D. Raybold, and A. Brown, Metal Powder Report Vol. 41, No. 4 (1986).

2. A.G. Revesz and J. Kruger in Passivity of Metals, R.P. Frankenthal and J. Kruger, Eds., The Electrochemical Society, Princeton, N.J. (1978) p. 137.

3. J. Stohr, D. Denley, and P. Persetti, Phys. Rev. B., 18 (1978) 4132.

4. G.G. Long, J. Kruger, D.R. Black, and M. Kuriyama, J. Electroanal. Chem., 150 (1983) 603.

5. R. Barchewitz, M. Cremonese-Visicato and G. Onori, J. Phys. C: Sol. St. Phys. 11 (1978) 4439.

6. V. Rehn in Low Energy X-Ray Diagnostics, D.T. Attwood and B. L. Henke, Eds., AIP Conf. Proc. No. 75, A.I.P., New York (1981) p. 162.

7. A.H. Compton and S.K. Allison, X-Rays in Theory and Experiment, 2nd Ed., Van Nostrand, Princeton, New Jersey (1935) Chap. 4.

8. M.A. Blokhin, The Physics of X-Rays, 2nd Ed., State Publishing House of Technical-Theoretical Literature, Moscow (1957) Chap. 5.

9. B.X. Yang, J. Kirz and I. McNulty, SPIE Proc. 689 (1986) 34.

10. R.W. Wood, Phil. Mag. 4 (1902) 396.

11. B.X. Yang, J. Kirz and S. Xu, to be published.

Table 1 - Fitting Parameters, Oxygen K-edge EXAFS

-----	E_o	σ_1	N_1	r_1 (nm)	σ_2	N_2	r_2 (nm)
MgO single crystal	-5	0.089	2.3	0.204	0.125	9.1	0.286
Thin film on AZ61	-13.5	0.148	2.5	0.203	0.189	6.5	0.288

FIGURE CAPTIONS

Fig. 1 The reflectance, R, as a function of the normalized glancing angle, ϕ/ϕ_c, for different values of β/δ.

Fig. 2 Penetration depth in MgO as a function of grazing angle, ϕ, for a range of energies.

Fig. 3 Reflectance measurements on single crystal MgO for reflection angles between 1.5 and 3 degrees.

Fig. 4 Geometry of the reflEXAFS surface reflectivity measurements.

Fig. 5 The EXAFS function (multiplied by k^2) extracted from the reflEXAFS curve measured at 1.5 on an MgO single crystal.

Fig. 6 The EXAFS function (multiplied by k^2) extracted from the reflEXAFS curve measured at 1.5 on a film on pure Mg.

Fig. 7 The EXAFS function (multiplied by k^2) extracted from the reflEXAFS curve measured at 1.5 on a film on AZ61.

Fig. 8 The magnitude of the Fourier transform calculated from the data shown in Fig. 5.

Fig. 9 The magnitude of the Fourier transform calculated from the data shown in Fig. 6.

Fig. 10 The magnitude of the Fourier transform calculated from the data shown in Fig. 7.

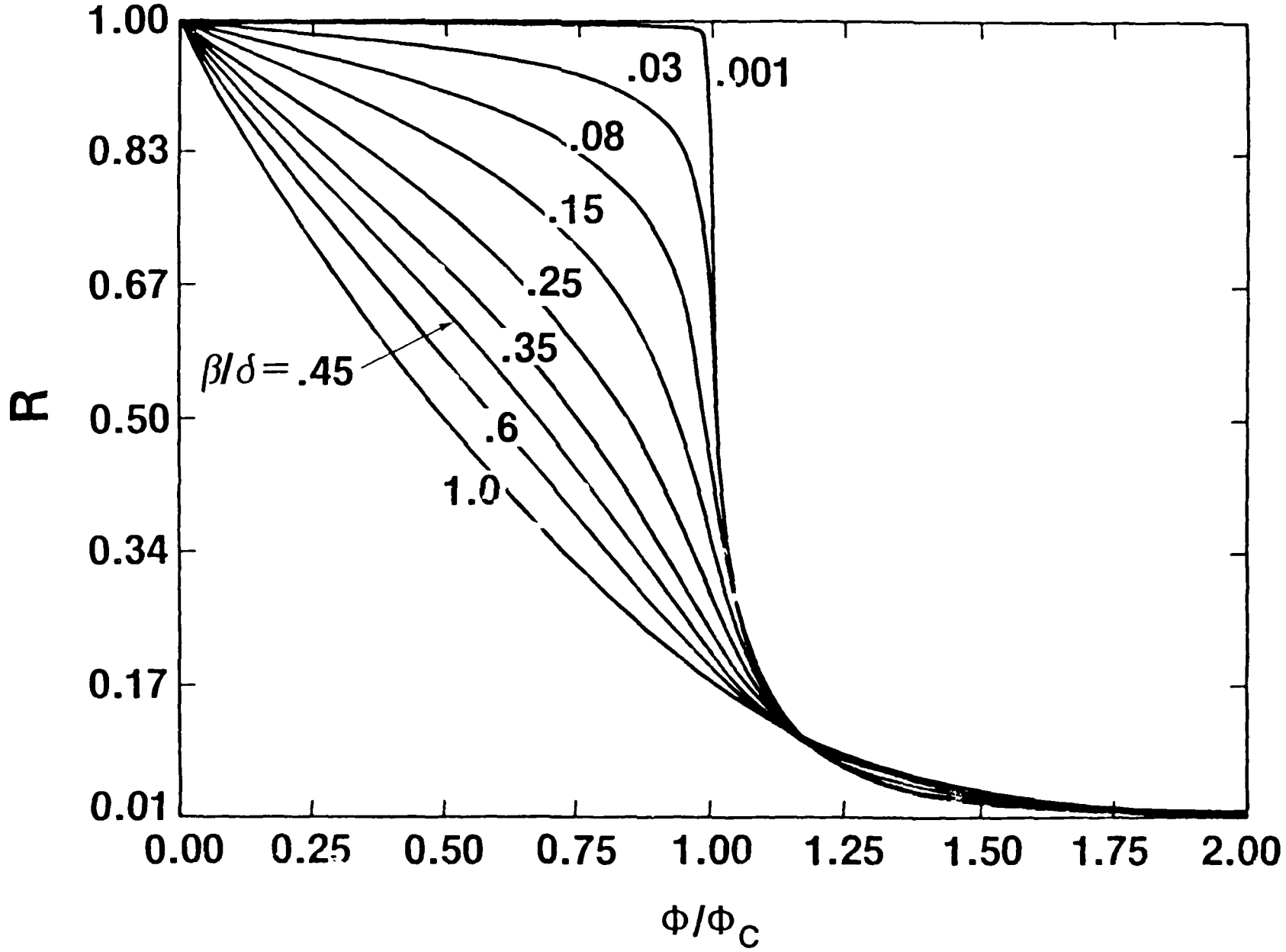
1.00
0.83
0.67
0.50
0.34
0.17
0.01
R
.03
.001
.08
.15
.25
.35
.6
1.0
β/δ = .45
0.00
0.25
0.50
0.75
1.00
1.25
1.50
1.75
2.00
Φ/Φc

Figure 1

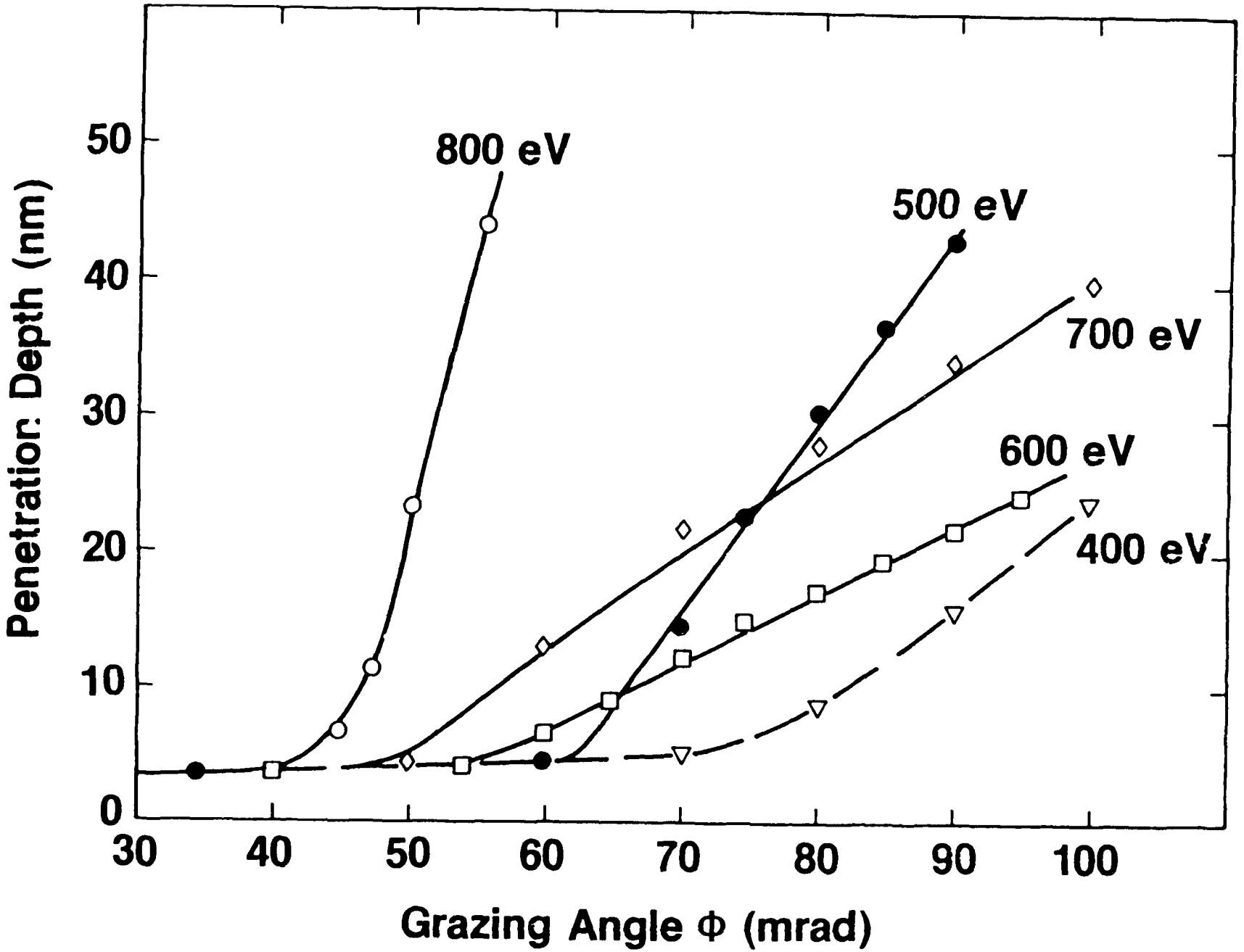
800 eV
500 eV
700 eV
600 eV
400 eV
Penetration Depth (nm)
0
10
20
30
40
50
30
40
50
60
70
80
90
100
Grazing Angle Φ (mrad)

Figure 2

refIEXAFS Geometry

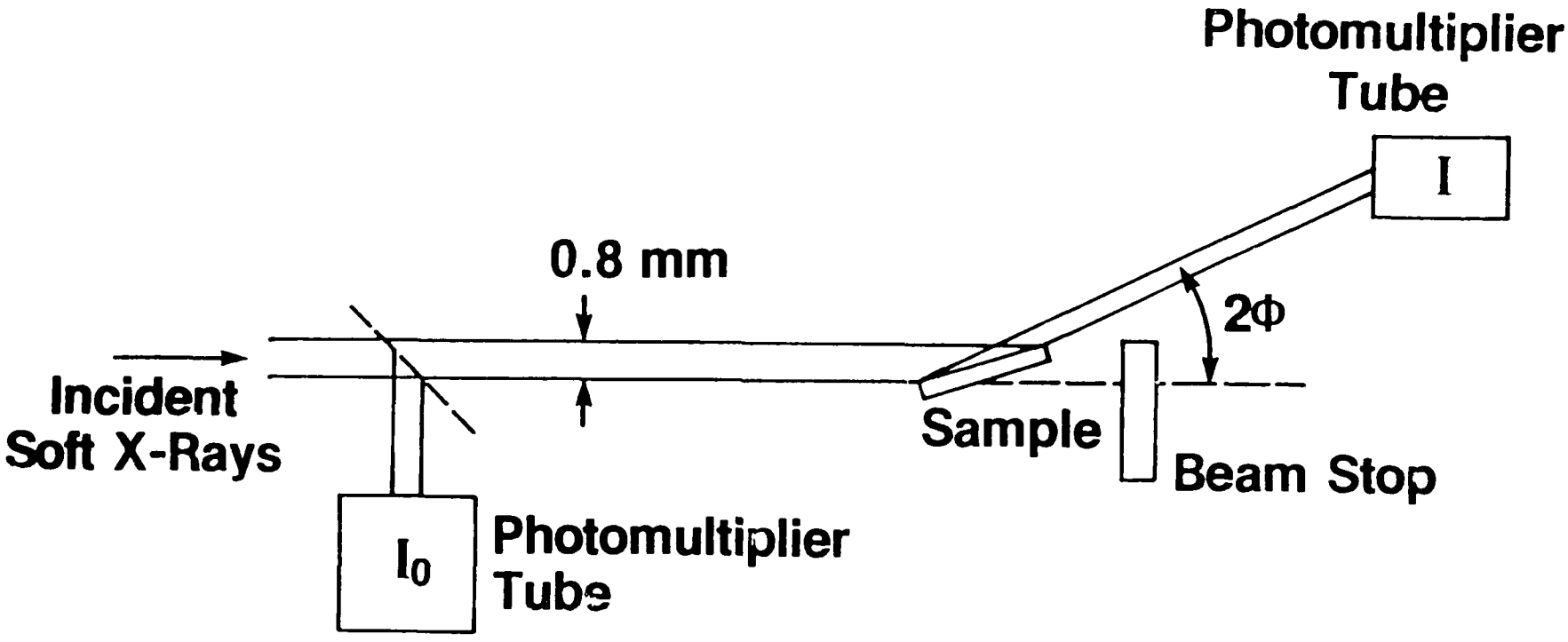

Figure 3

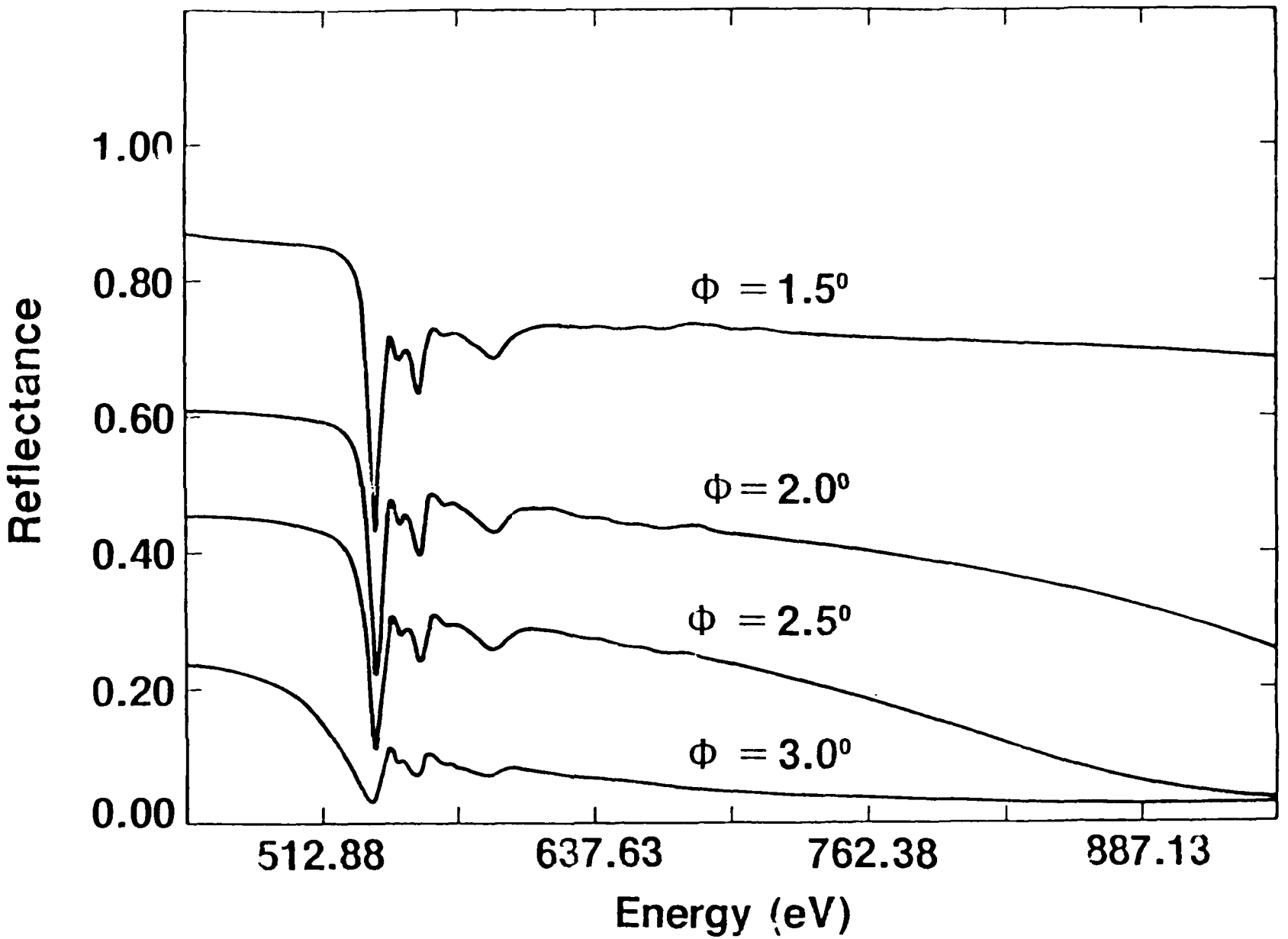
1.00
0.80
0.60
0.40
0.20
0.00
Reflectance
Φ = 1.5°
Φ = 2.0°
Φ = 2.5°
Φ = 3.0°
512.88
637.63
762.38
887.13
Energy (eV)

Figure 4

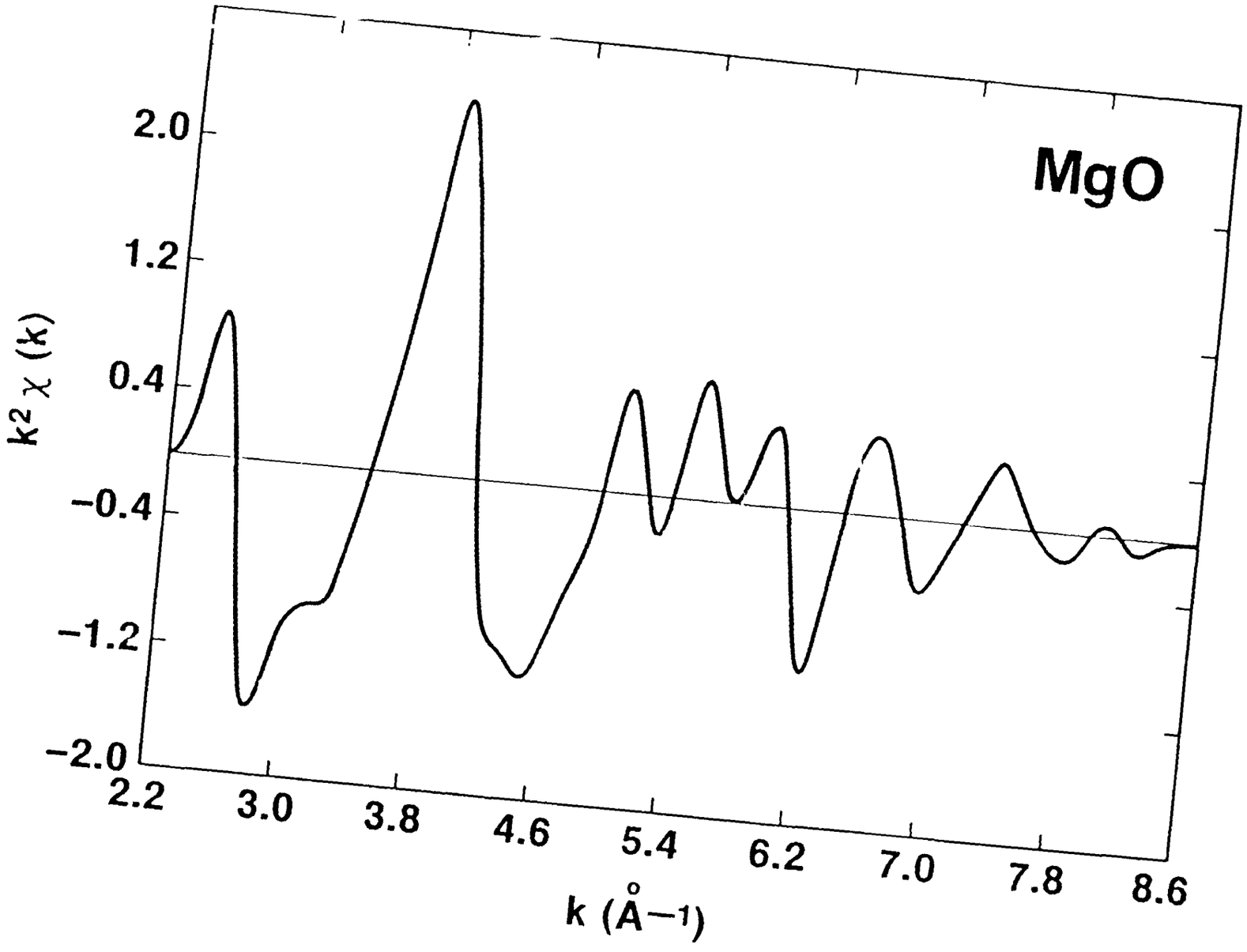

Figure 5

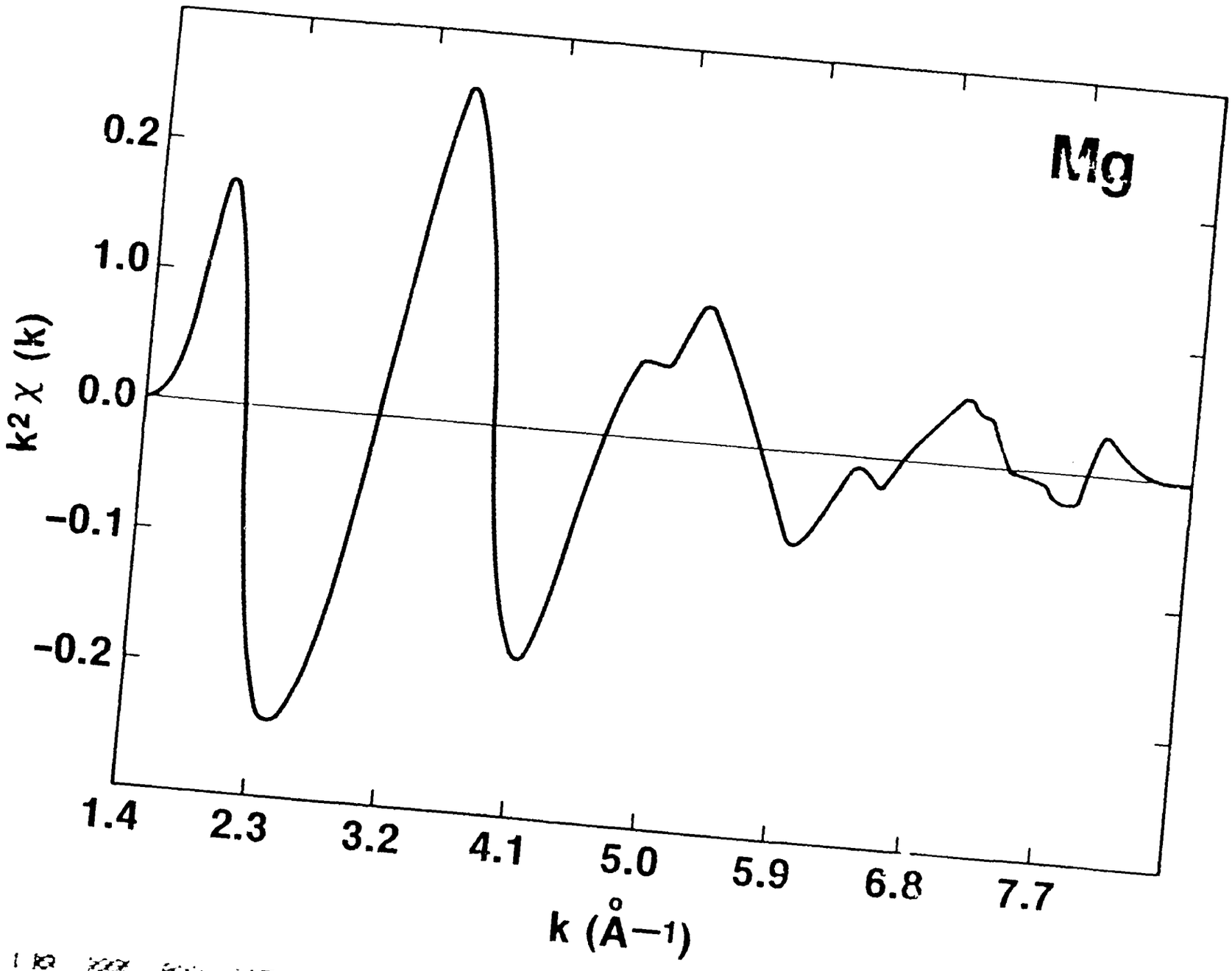

Figure 6

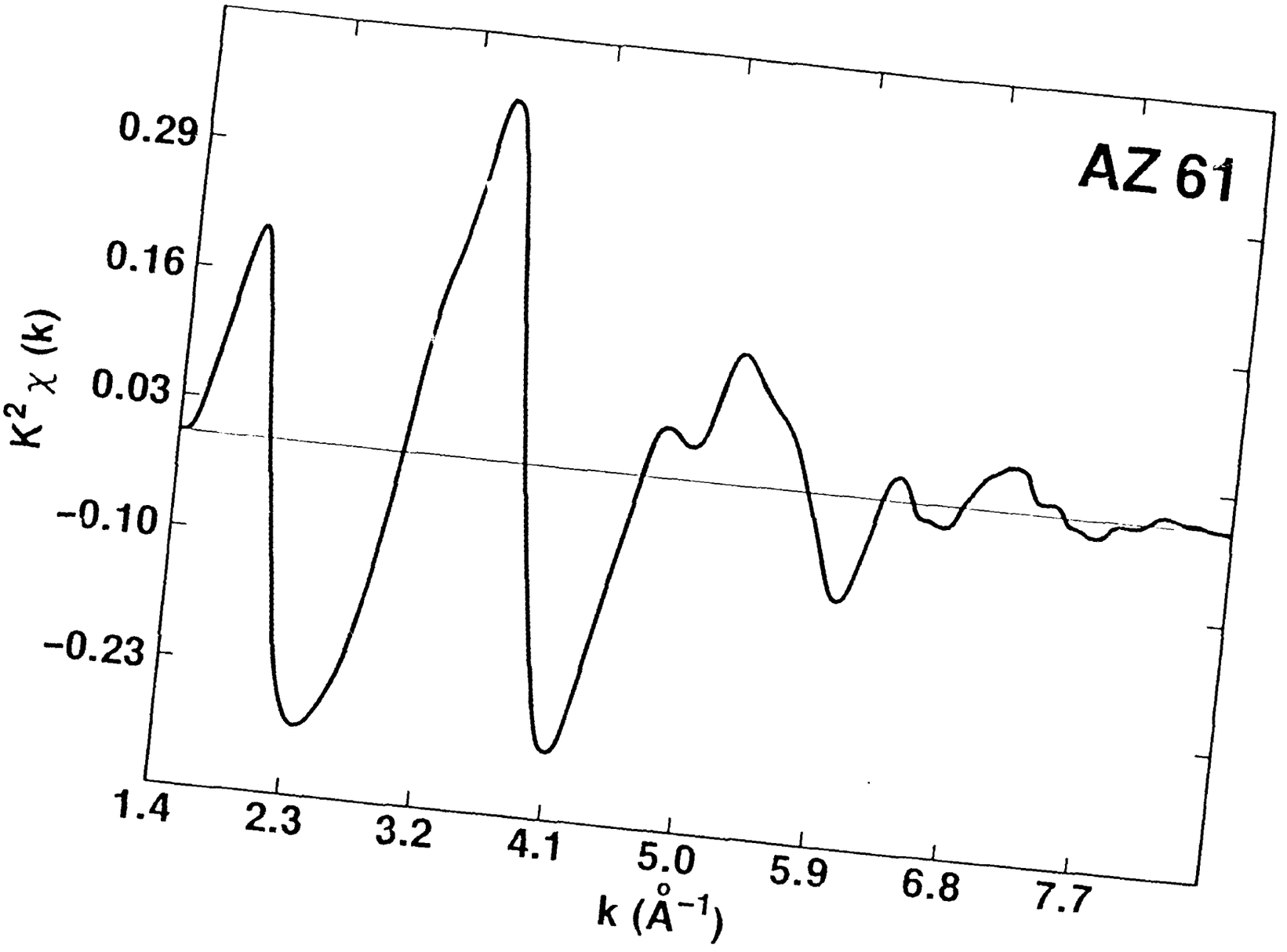

Figure 7

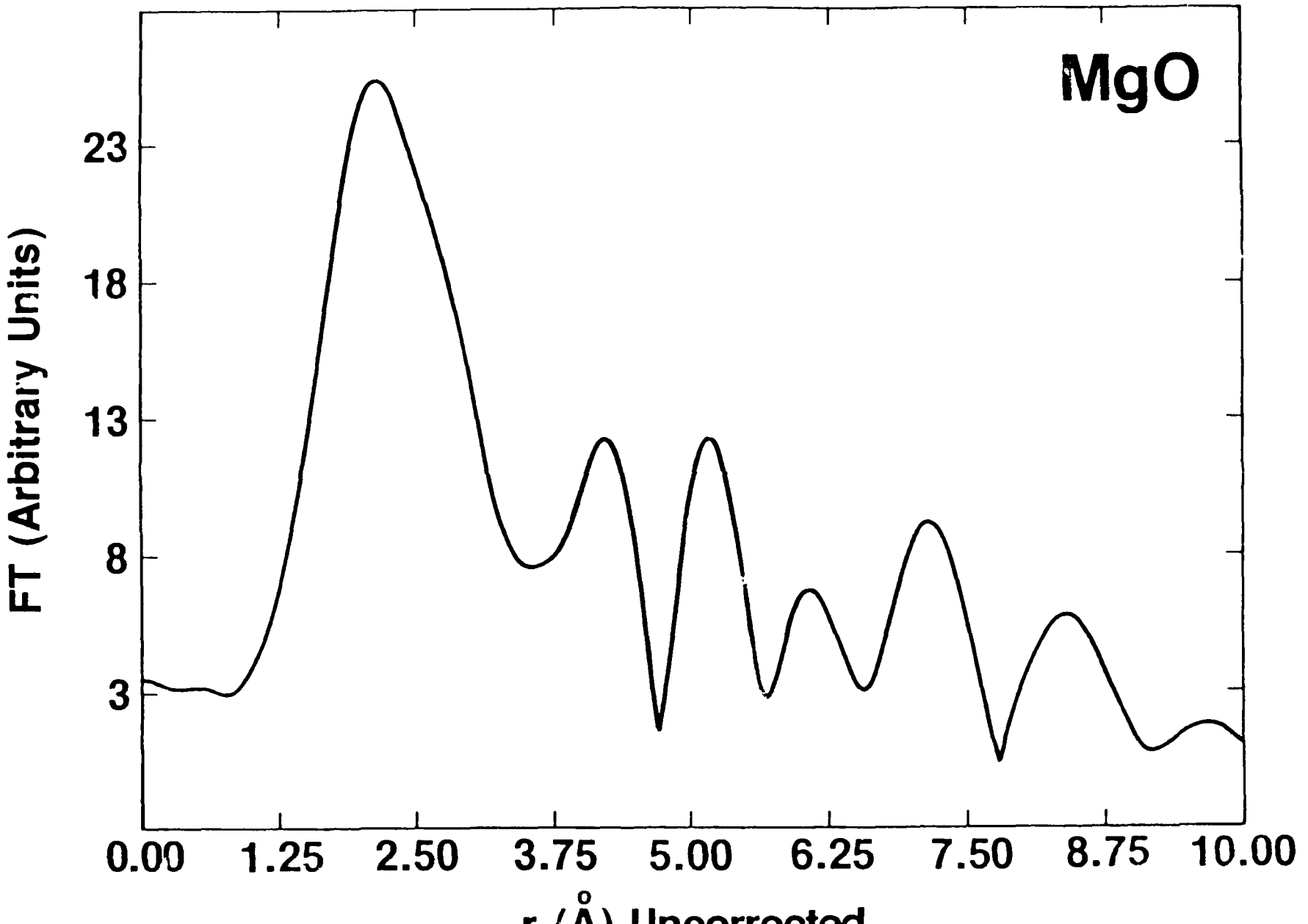
MgO
FT (Arbitrary Units)
23
18
13
8
3
0.00
1.25
2.50
3.75
5.00
6.25
7.50
8.75
10.00
r (Å) Uncorrected

Figure 8

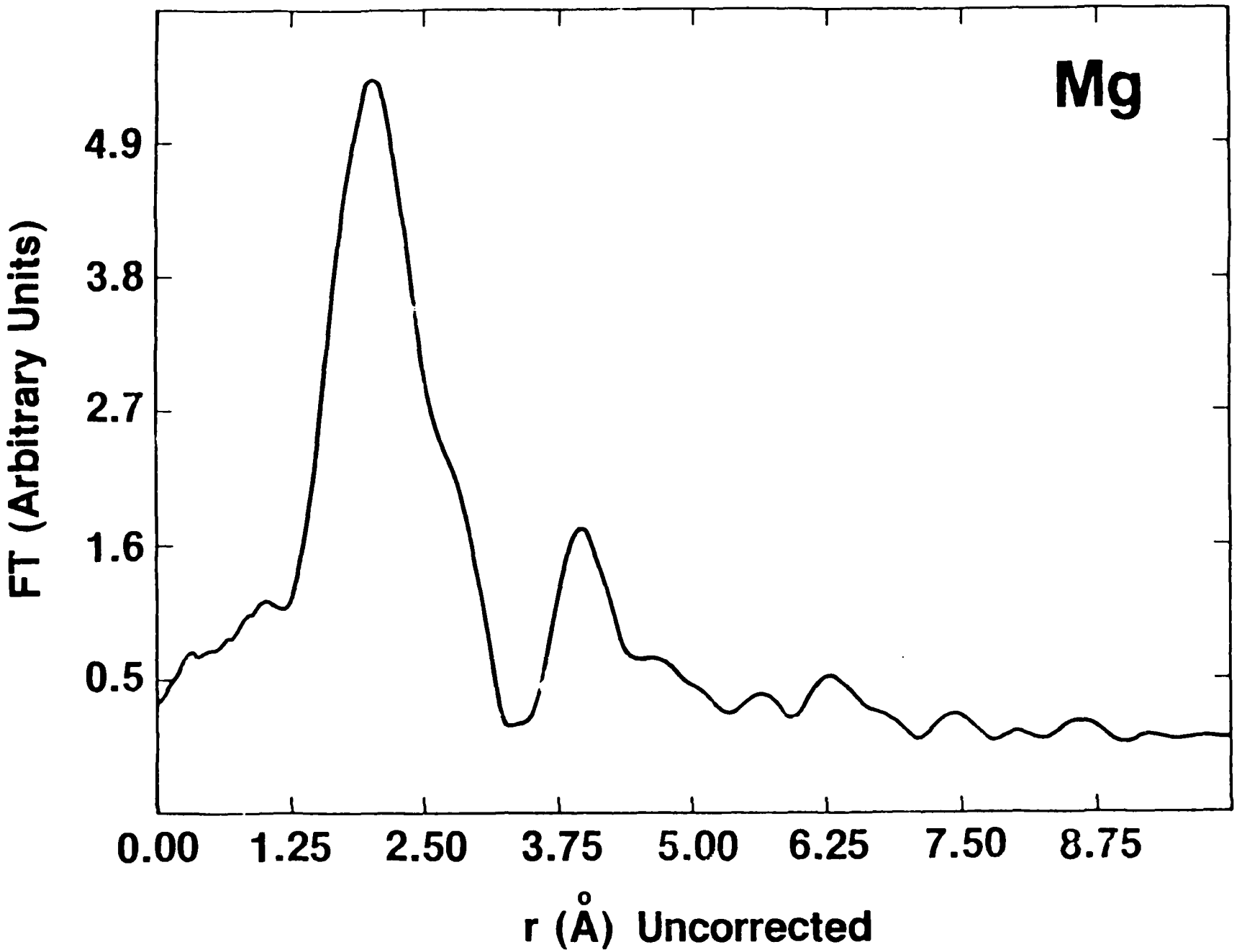
Mg
FT (Arbitrary Units)
4.9
3.8
2.7
1.6
0.5
0.00
1.25
2.50
3.75
5.00
6.25
7.50
8.75
r (Å) Uncorrected

Figure 9

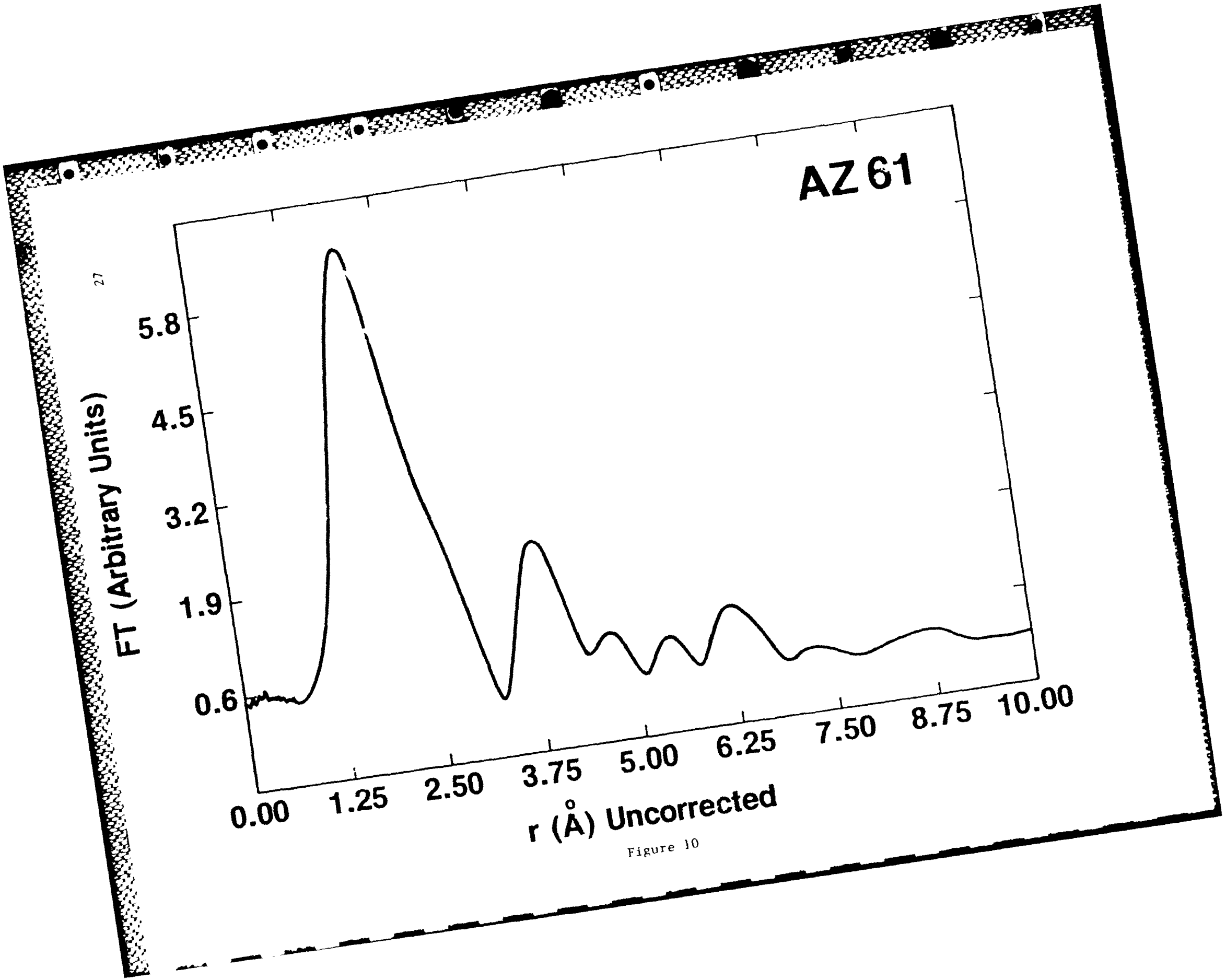
AZ 61
FT (Arbitrary Units)
5.8
4.5
3.2
1.9
0.6
0.00
1.25
2.50
3.75
5.00
6.25
7.50
8.75
10.00
r (Å) Uncorrected

Figure 10

PART II--An expanded and revised version of this part will be submitted to Corrosion.

Corrosion of Rapidly Solidified Mg Alloys

G.L. Makar and J. Kruger
The Johns Hopkins University
Corrosion and Electrochemistry Research Laboratory
Baltimore, MD 21218

Electrochemical Impedance Spectroscopy (EIS) and other electrochemical techniques have been applied to study of the role of alloying and rapid solidification processing (RSP) on the corrosion of Mg alloys which have potential aerospace applications. EIS has been mainly used because it is a powerful electrochemical technique having the following attributes: 1) It is a non-destructive method of rapidly determining a uniform corrosion rate; 2) The raw data include quantification of the electrolyte resistance, a parameter which may cause underestimation of the calculated corrosion rate when not compensated for; and 3) It can provide mechanistic information. In this study EIS is used primarily to measure corrosion rates for the purpose of evaluating the effects of alloying elements. Future EIS work will extract fundamental information concerning the corrosion processes on the RS magnesium alloys, such as the roles played by Cl^- and H^+.

Nyquist presentations of impedance spectra, such as that shown for pure Mg in 0.05 M sodium borate in Figure 1, were used in this study to provide a rapid means for calculating corrosion rates. In such a format, the negative

imaginary component of the impedance, -Z'', is plotted against the real component, Z'. The semicircle generated in this quadrant represents a capacitive process, characteristic of a freely-corroding bare metal surface. The diameter of this semicircle is equal to the polarization resistance, R_p, which is inversely proportional to the corrosion rate. The intercept with the real axis at high frequency (that nearest the origin) defines the electrolyte resistance. A portion of the last year's work focused on establishing the accuracy of this method for measuring corrosion rates by comparing actual weight-loss values with those predicted by EIS. Table 1 shows the results of these studies for several cast alloys and pure magnesium.

As indicated in Table 1, the electrochemically-determined corrosion rates are quite accurate except in the case of pure Mg, for which the corrosion rate was underestimated by more than an order of magnitude. Visual inspection and Scanning Electron Microscopy (SEM) showed that the attack on the alloys was much different than that on the pure metal. Figures 2, 3, and 4 are SEM photomicrographs of pure Mg, cast AZ61, and RS AZ61, respectively, after exposure to 0.05M sodium borate and subsequent cleaning to remove the corrosion products. Notice that the attack on the cast and RS AZ61 is much more uniform than that on the pure magnesium. A closer examination of the pure Mg surface reveals evidence of the so-called "chunk effect," whereby particles are removed by an undermining

process. The loss of these particles, such as the one seen in Figure 5, are not recorded electrochemically, causing techniques such as EIS to underestimate the true rate of metal loss. The rapidly solidified alloys which are the object of this study corroded very uniformly, implying that the corrosion rates measured using electrochemical methods are accurate.

Based on EIS measurements of corrosion rates in 0.05 M sodium borate, several preliminary conclusions may be drawn regarding alloying additions examined thus far. Aluminum clearly is the most effective in promoting very low corrosion rates, almost certainly due to its ability to form stable oxides. Studies of binary Mg-Al alloy indicate that the corrosion rate decreases with increasing Al content; however, the amount of aluminum added will be limited by the embrittling effect of $Mg_{17}Al_{12}$. Cerium also appears to form a corrosion-resistant phase. An alloy found to have a cerium-enriched surface also had a relatively low corrosion rate. Corrosion rates of binary and multicomponent alloys containing zinc suggest that small additions may have a beneficial effect on corrosion resistance. This possibility, coupled with its strengthening effects, makes zinc a desirable alloying element.

Based on the performance of multicomponent melt-spun ribbons containing neodymium and yttrium, these elements are not attractive for further study. However, bulk alloys obtained from Allied Signal Corp. containing these elements

had corrosion rates approximately equal to that of AZ61. These alloys were either in the as-cast condition or extruded from RS particulate. These materials have good mechanical properties and very low corrosion rates in unbuffered chloride-containing aqueous solutions (1), indicating that they deserve further study.

Lithium also appears to warrant further study. The corrosion behavior of magnesium alloys is not adversely affected by small (0.2 wt.%) additions, while Li has the advantage of very low density.

Manganese additions seem unnecessary for RS Mg alloys. No benefits of Mn additions were apparent in the multicomponent alloys, and the corrosion rates of Mg-Mn binary alloys were very high. The accepted role of manganese in cast magnesium alloys is to tie up impurity elements in less harmful phases, most notably iron. It is likely that the more favorable distribution of alloying and impurity elements achieved by RSP makes Mn additions unnecessary. Calcium appears to be detrimental to corrosion performance even in the 0.8 wt.% range and is not attractive for further study.

The effect of RSP on AZ61 was investigated by conducting anodic polarization studies in the presence of chloride. The electrolytes used were 0.05 M Na borate (pH 9.2) or 0.025 M Na carbonate/0.025 M Na bicarbonate (pH 10.0) with 100 ppm, 1000 ppm, or 3.5 % NaCl. Figure 6 presents anodic scans for cast and RS AZ61 in the carbonate

buffer with 100 ppm NaCl. The characteristic parameters i_p and E_b are indicated. The passive current density, i_p, is a measure of the protective film's ability to maintain a low corrosion rate in the passive regime. The breakdown potential, E_b, is one measure of a metal's resistance to attack by an aggressive species; a higher (more positive) value of E_b, indicates better resistance. Previous studies (2) revealed that i_p and open-circuit dissolution rate was affected little by RSP Mg. Resistance to Cl^- attack, however, shows some interesting improvements.

Figure 7 shows that the breakdown potential for the RS AZ61 is about 200 mV higher than that for the cast material. This 200 mV improvement was observed in the carbonate buffer at all Cl^- levels. Figure 7 presents the results of similar experiments conducted in the borate buffer with 100 ppm NaCl. The breakdown potentials do not indicate any improvement for the RS material, which was the case for all chloride levels. However, the region of the curve for the cast material marked "x" in Figure 8 indicates a pitting event followed by repassivation. These pits were also observed visually, and hydrogen was seen to evolve from them at a very low rate during the balance of the experiment. The implication is that the borate-formed film more readily nucleates pits and is probably less stable on the cast AZ61. These improvements may be a result of increased homogeneity or the promotion of glassy films, possibly a combination of both.

Future electrochemical studies have as their goal a closer examination of these possible synergistic effects of alloying elements and rapid solidification. Especially of interest is the ability of these materials to resist attack by chloride, and so studies will focus on evaluating effects such as passive film stability and the resistance to breakdown/repassivation events as measured by electrochemical noise techniques. Electrochemistry will also be combined with ellipsometry in order to evaluate film growth kinetics.

Acknowledgment

We are grateful to Dr. Patrick Hagans for his most valuable contributions to these studies.

References

(1) C.F. Chang, S.K. Das, D. Raybould, and A. Brown, Metal Powder Report, Vol. 41, No. 4, April, 1986.

(2) J. Kruger, G.G. Long, and D.K. Tanaka, First Annual Report, Johns Hopkins University, F4966620-86-C-00014,P00002 Air Force Office of Scientific Research, Nov. 26, 1986.

Table 1 - Corrosion-Rate Measurements, Electrochemical vs. Gravimetric

Material	Corrosion Rate, mpy		
--------	EIS	Pol. Resist.	Gravimetric
Cast AZ61	130	120	110
Cast Mg-30Al	47		42
Alloy 5066	120	110	125
Alloy 5090	140	110	100
Pure Mg	50	50	640

Nyquist Presentation

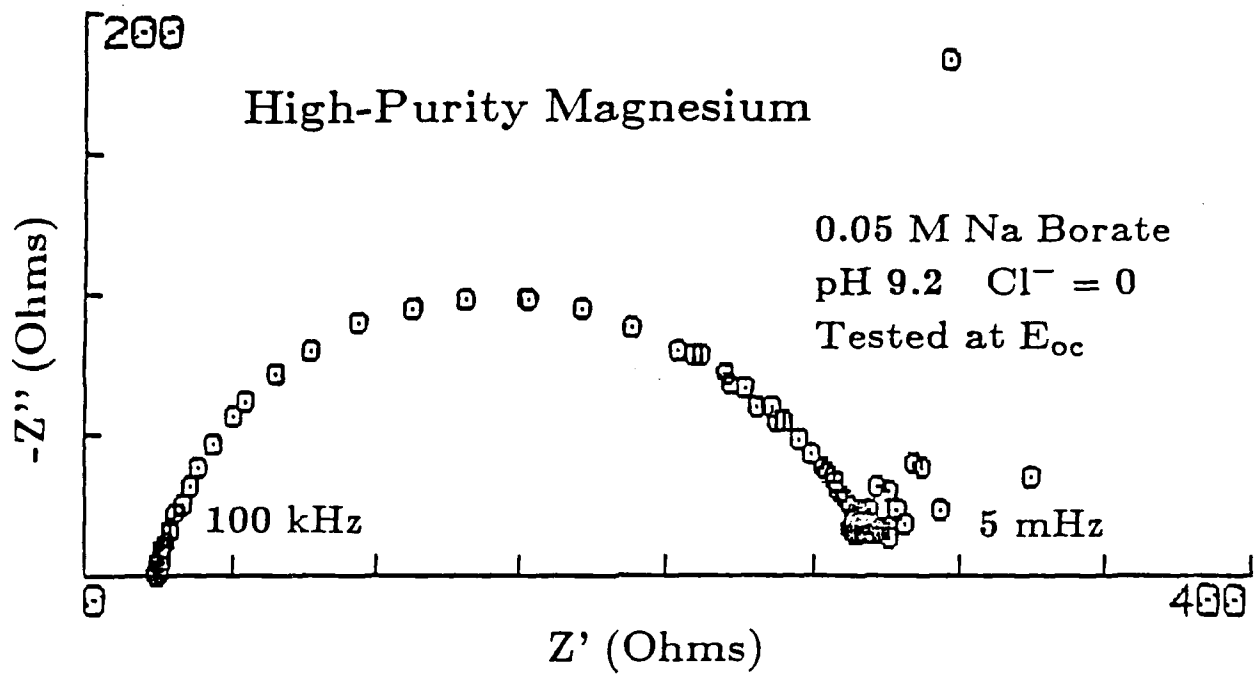

Figure 1

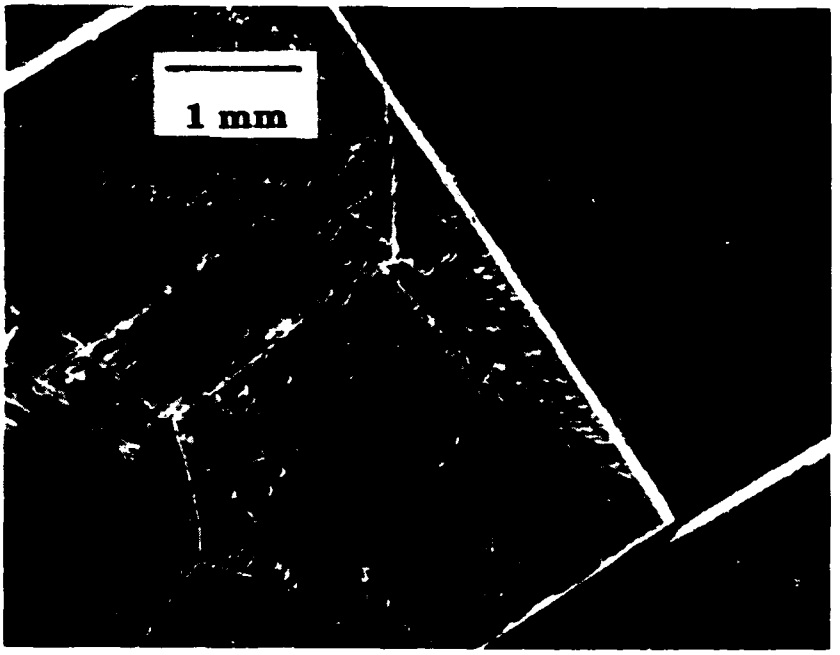

Figure 2

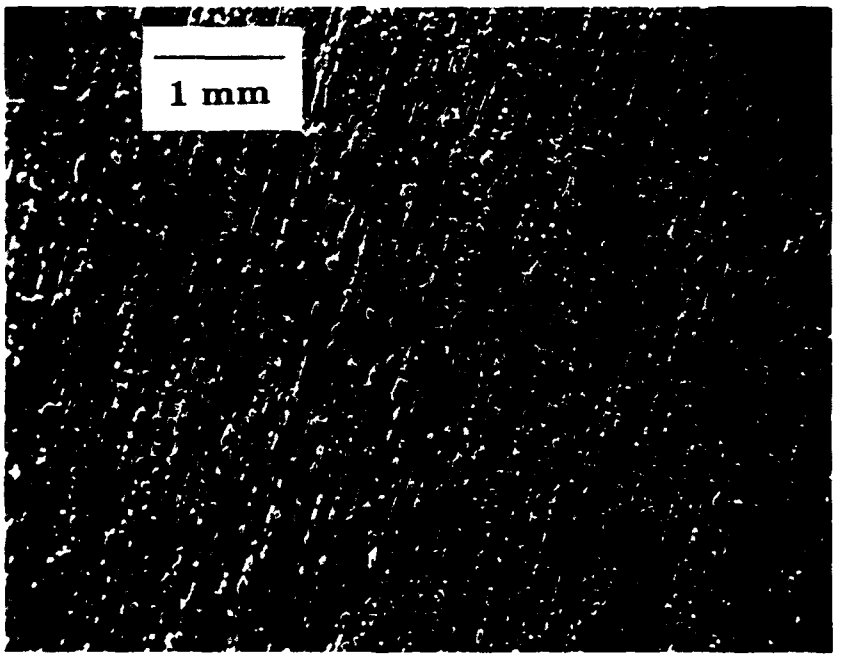

Figure 3

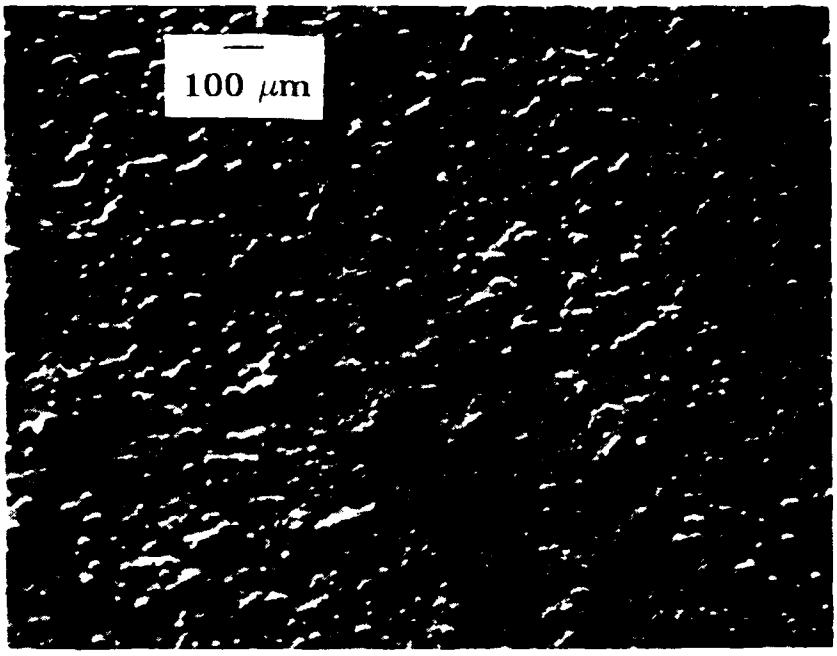
100 μm

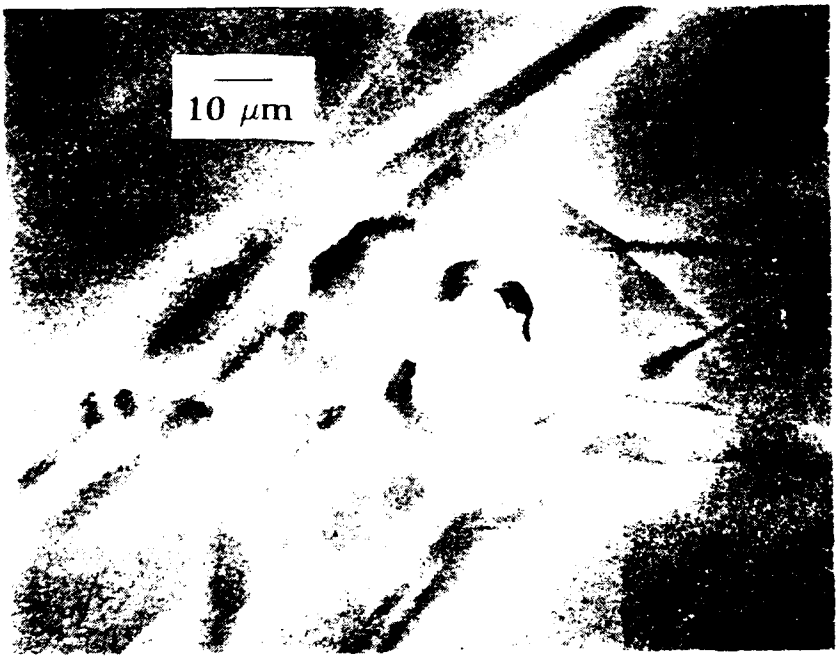
10 μm

Anodic Polarization

AZ61 - 100 ppm NaCl

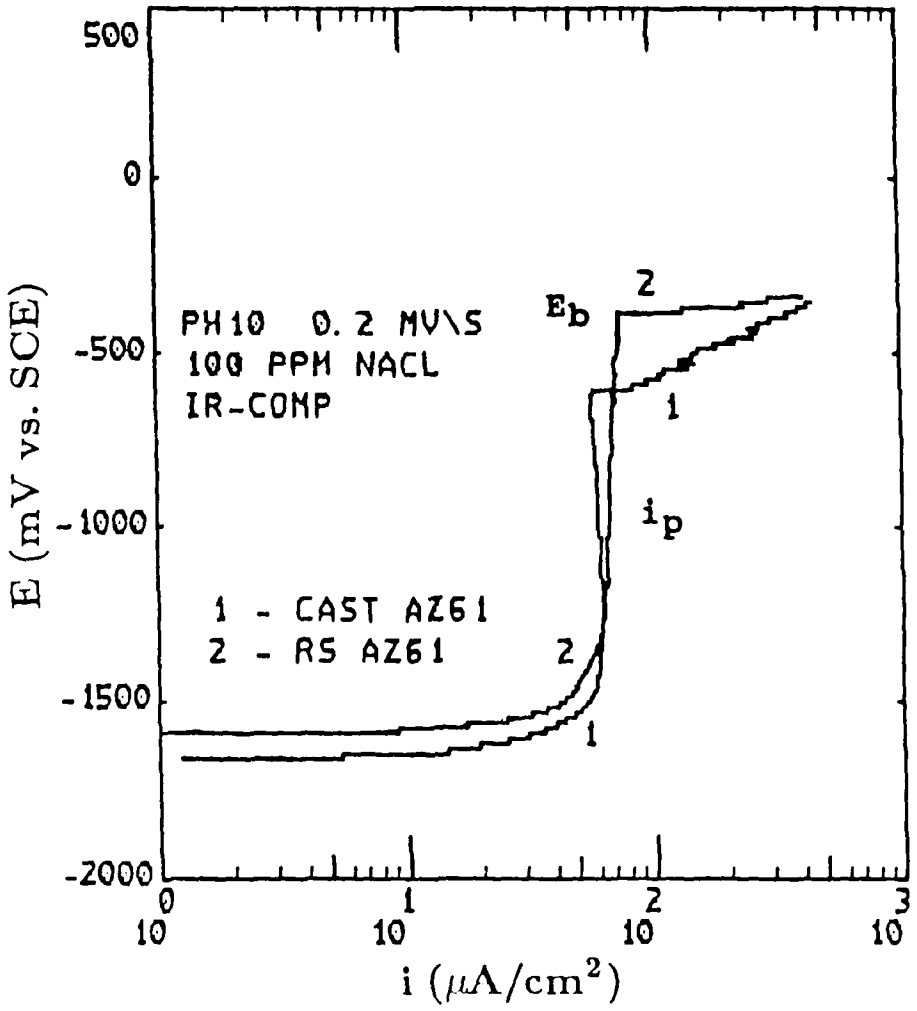

Figure 6

Anodic Polarization

AZ61 - 100 ppm NaCl

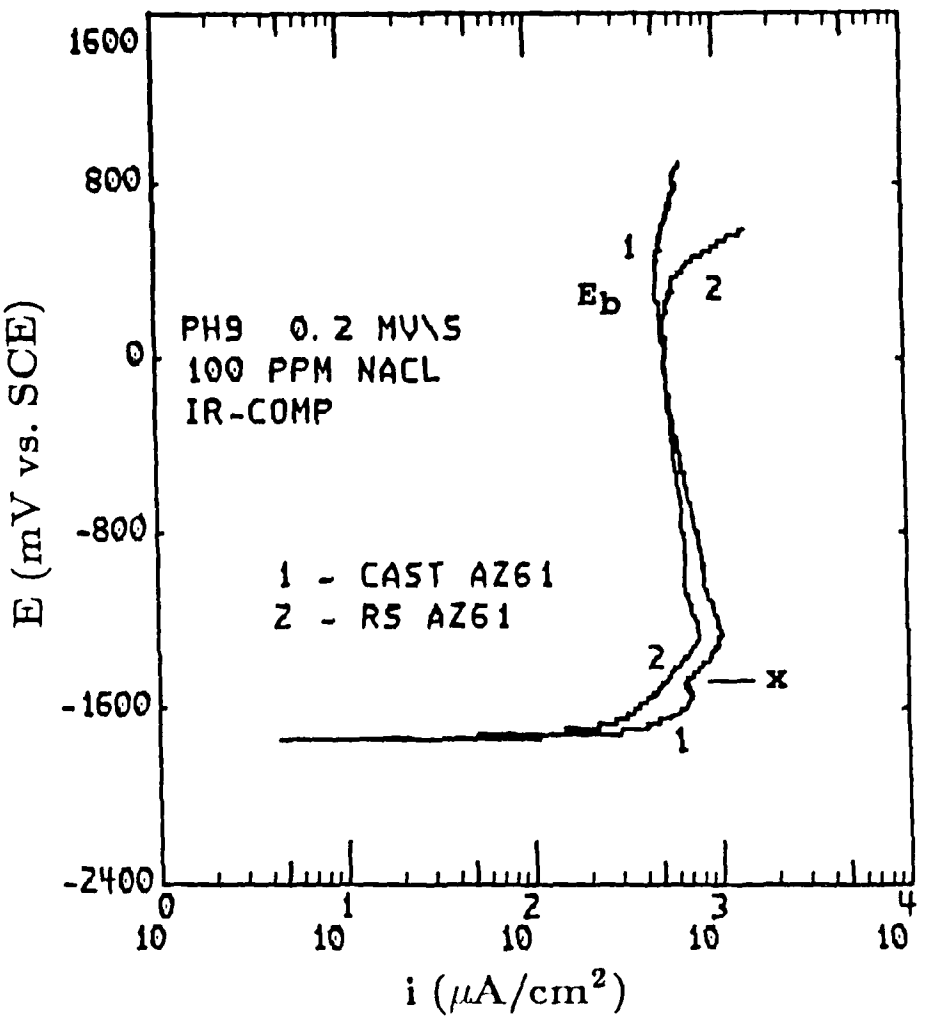

Figure 7

PART III Report from sub-contractor, Lockheed Palo Alto Research Laboratory

MATERIALS PREPARATION

&

CHARACTERIZATION OF RSP MAGNESIUM ALLOYS

Final Report

For period January 1, 1987 - October 30, 1987

Contract PO # 8604-51292-X

Prepared by

A. Joshi
Dept. 93-10, Building 204
Lockheed Palo Alto Research Laboratory
3251 Hanover Street
Palo Alto, CA 94304

to

The Johns Hopkins University
Baltimore, MD 21218

CONTENTS

List of figures

List of Tables

1. INTRODUCTION

Materials preparation and characterization support is provided to Johns Hopkins University (JHU) under this contract, in support of their activities under the JHU contract F496620-86-C-0014, P00002, entitled "A Fundamental Understanding of the Effect of Alloying Elements on the Corrosion Resistance of Rapidly Solidified Magnesium Alloys", funded by the Air Force Office of Scientific Research.

The purpose of the characterization task is to understand the nature, specifically the structure and chemistry, of passive films that form on surfaces of magnesium alloys and thereby contribute to the elucidation of the corrosion mechanisms. In order to achieve these objectives high purity binary alloys were prepared and selected alloys with unusual corrosion behavior were characterized utilizing the surface analytical techniques. In addition, a multicomponent alloy was evaluated to determine the role of key alloying elements on the surface film formation. This report discusses the preparation of binary alloys, corrosion studies and characterization activity performed on Mg-Zn alloy system, a Mg-Al alloy and a Mg-Al-Li-Zn-Mn-Ce multicomponent alloy.

2. MATERIALS PREPARATION

Several of the binary rapidly solidified (RS) magnesium alloys and the multicomponent alloy used in this study were originally prepared under the AFWAL-funded program "Rapidly Solidified Magnesium alloys". Mg-9.35 wt% Zn alloy was prepared under the LMSC IRAD "Thin Film Structures", task "Passive Films". The procedures followed in preparation of these alloys are outlined briefly in this section.

2.1. Preparation of Binary Alloys: All the binary alloys were prepared in approximately 200 g quantities utilizing high purity starting materials. All the alloys were induction melted in tantalum crucibles of 0.225 mm (0.009 in) wall thickness, surrounded by a 3.17 mm (0.125 in.) thick wall iron susceptor. Melting was carried out in argon gas at 1 atmosphere absolute pressure. Temperature measurements were made with a chromel-alumel thermocouple contained in a BeO sleeve. After holding at the high temperature for the desired period, typically 6 to 10 minutes at temperatures above 650°C to assure solution of the alloying elements, the melt was agitated by rocking the crucible for at least 30 seconds and poured into a segmented copper mold 12.7 mm thick x 10.2 cm wide x 15.2 cm high (0.5 in. X 4 in. X 6 in.) held near room temperature (not water cooled). No reaction of the molten metal was observed with the liner, crucible, thermocouple, or mold material. The casting surfaces contained no abnormal surface oxides and possessed metallic luster. Table I shows the compositions of the alloys used in this investigation.

2.2 Rapid Solidification of Binary Alloys: RS materials could be prepared by a number of techniques and two of them were considered as primary candidates for utilization in these studies. Both techniques, the preparation of splat specimens and melt spun ribbons, offer sufficient flexibility and permit preparation of small amounts of experimental materials needed for characterization purposes. Typically, the splat specimens could be prepared utilizing high cooling rates of the order of 10^6K/sec, thereby allowing further exploration of RS benefits. In comparison, melt spinning, which typically provides cooling rates of the order of 10^5K/sec, can achieve a material that is more uniform in composition and microstructure, an advantage for obtaining reliable corrosion and characterization data. Mainly for this reason, all the RS activity was conducted using melt spinning.

A small scale melt spinner at the Gaithersburg, Maryland, facilities of the National Bureau of Standards (NBS) was used in preparing all the melt spun ribbons. Typically 1 to 5 g of the material is prepared for each alloy, which is adequate to carry out property evaluations in ribbon form.

Typical procedure in making a melt spinning run involved the following steps:

1. The crucible is loaded with an appropriate amount (1 to 5 g) of previously cast magnesium alloy.
2. The chamber is evacuated to a relatively low pressure (10^{-4} torr) and pressurized with inert gas (helium). The absolute pressure in the chamber is maintained at 69 MPa (10 psia) and 96.5 MPa (14 psia) in the crucible.
3. The alloy is melted with an induction heating power supply, which typically takes 35-40 seconds. Melting is observed through a view port at the top of the crucible.
4. The induction power is continued until the desired superheat is achieved. A 4 to 5 seconds of power input after the melting point is reached, is estimated as equivalent to a superheat of 50 to 100°C.
5. The pressure activator is triggered to stream the molten metal on to the spinning wheel. The pressure activator admits helium gas into the crucible and pressurizes it to 138 MPa (20 psia).

An uncoated tantalum crucible, which exhibited no reaction with any of the magnesium alloys, was utilized in preparation of most of these alloys. The crucible was cleaned or a new one substituted every time a new alloy is prepared, in order to avoid contamination.

3. CORROSION STUDIES

Corrosion rates of all the binary alloys were determined earlier at Johns Hopkins University (under the AFWAL program) using ELectrochemical Impedance Spectroscopy (EIS). An electrolyte containing 0.05 M sodium borate with a pH of 9.2 was employed. Two graphite rods served as counter electrodes, and a saturated calomel electrode (SCE) was used as a reference. Typically measurements were conducted on the free surface of the ribbon after the surface is allowed to establish a steady-state open-circuit potential for about one hour. The results of these measurements with corrosion rates expressed in mils per year are shown in Fig. 1. As evidenced, only aluminum at relatively high concentrations appears to have a significant positive impact on the corrosion rates. Characterization of the electrochemically corroded surfaces is likely to provide information about the surface film formation, if any. It was also interesting to note the Mg-Zn alloys exhibited a significant (Mg-Ca alloys to a lesser degree) drop in corrosion rate at high solute concentrations. An understanding of why the corrosion rate as a function of solute concentration is increased at low concentrations and decreased at high concentrations is likely to provide insights into passive film formation. Mg-Zn system is selected for extensive corrosion evaluations also because of the key role played by zinc as a potent solid solution strengthener in magnesium.

Corrosion studies in the present program included evaluation of the role of zinc in magnesium, the role of quench rate and other factors as differentiated at the free surface and wheel contact surface, and the role of exposure time in the electrolyte. Mg-Zn alloy system is utilized in all these studies. In addition, progress on Mg-14.4 wt% Al alloy in understanding the surface compositional differences among the two ribbon surfaces and the role of prior chemical etching on the corrosion behavior is included. The role of alloy composition as it affects the chemistry and corrosion behavior of the two sides of the ribbon and influence of chemical etching are being studied utilizing the multicomponent alloy 15.

In preliminary studies it was noted that the corrosion rate determined by EIS has a strong dependence on the time of exposure in the sodium borate solution to establish open-circuit potential. In order to understand this phenomenon, corrosion rates were determined on Mg-Zn alloys after they were exposed for 20 minutes and 60 minutes in the solution. The results obtained from both surfaces of these alloys are shown in Table II. The results indicate little or no effect of exposure time on high purity RS magnesium, but a strong influence in zinc containing alloys. Longer exposure time resulted in a significant increase in corrosion rates on both sides of the ribbon. For a given exposure time the wheel contact surface corroded at a faster rate than the free surface. In all cases, the general behavior indicating highest corrosion rate for the Mg-9.35 wt% Zn alloy remained prominent (Fig.2).

4. MATERIALS CHARACTERIZATION

Surface chemistry modifications resulting from exposure to electrolyte and the films formed upon chemical etching were evaluated utilizing Auger Electron Spectroscopy (AES) and x-ray photoelectron spectroscopy (XPS). AES studies were instrumental in providing the surface and in-depth compositional information, while XPS was utilized to provide detailed chemical state information. In some instances XPS profiling (in conjunction with ion sputtering) was conducted to obtain chemical state changes as a function of depth. The interpretation of these data shall be made with caution, as it is likely that energetic ions cause damage to the chemical state of surface atoms.

3.1. X-Ray Photoelectron Spectroscopy (XPS): The experimental technique in XPS, more commonly known as electron spectroscopy for chemical analysis (ESCA), involves excitation of a solid surface using monochromatic x-radiation and energy analysis of the ejected photoelectrons. MgK_α X-rays (1253.6 eV) or AlK_α X-rays (1486.6 eV) are ordinarily used. These photons have limited penetrating power in a solid, of the order of 1-10 micrometers. They interact with atoms in this surface region by the photoelectric effect, causing electrons to be emitted. The emitted electrons have kinetic energies given by: $KE = h\nu - BE - \phi_S$ where $h\nu$ is the energy of the photon, BE is the binding energy of the atomic orbital from which the electron originates, and ϕ_S is the spectrometer work function.

The binding energy may be regarded as an ionization energy of the atom for the particular shell involved. Since there is a variety of possible ions from each type of atom, there is a corresponding variety of kinetic energies of the emitted electrons. Moreover, there is a different probability, or cross-section for each process. In XPS, precise measurement of photoelectron energies and intensities is carried out using an electron spectrometer. The peaks in the measured electron energy distribution spectrum (electron intensity versus electron energy) represent specific binding states of electrons in individual surface atoms. Precise determination of peak positions often provides information of their chemical states, while peak intensities are used in calculating atomic concentrations. The high surface sensitivity of the technique arises primarily due to short escape lengths of electrons emerging from the solid. Probabilities of interaction of the electrons with matter far exceed those of the photons, so while the path length of the photons is of the order of micrometers, that of the electrons is of the order of tens of Angstroms. Thus, while ionization occurs to a depth of a few micrometers, only those electrons that originate within tens of Angstroms below the solid surface can leave the surface without energy loss. It is these electrons which produce the peaks in the spectra and are most useful. Those that undergo loss processes before emerging contribute to the background. The escape depth of electrons is in the 5-25 Å range for most metals , and in the 5-100 Å range for most organic and biological substances.

An SSX-100 system manufactured by Surface Science Laboratories was utilized in gathering all the XPS data. The small spot capability permitted collecting XPS data from individual ribbon surfaces, which are typically only 2-3 mm wide. Minimum diameter of the x-ray beam in this system is 250μm, and a 600μm beam is typically employed in these studies.

4.2 Auger Electron Spectroscopy: When a specimen is bombarded with energetic electrons (1 to 30 keV), both characteristic x-rays as well as characteristic electrons, named Auger electrons after the discoverer, Pierre Auger, are emitted. In AES, the energies of emitted electrons are precisely determined using an electron spectrometer and used to identify the specimen surface. The technique is highly surface sensitive, as these low energy electrons are emitted from a shallow region of order of 5 to 20Å. The technique has capability to detect all elements except hydrogen and helium and provides quantitative information with the help of external standards. The technique is often utilized to obtain highly localized information (using focused primary electron beams), surface chemical homogeneity information in the form of Auger elemental images, and depth-compositional information in conjunction with ion sputtering. For some elements chemical state may also be determined by observing small shifts in the Auger peaks due to chemical binding effects.

All the AES studies reported here were conducted using PHI 560 ESCA/SAM system manufactured by Perkin Elmer Corporation.
The surface analysis results obtained along with the corrosion information are discussed in the following section.

5. RESULTS AND DISCUSSIONS

5.1 Mg-Zn Alloys: The Mg-Zn alloys in the as-rapidly solidified condition have surface oxides in the 70-200Å range. The oxide is primarily magnesium rich, with little or no zinc present at the surface or within the oxide. In some cases, a small amount of silicon (contaminant) was observed at the surface. An example of the AES spectrum obtained from the wheel contact surface of the Mg-27.5 wt% Zn alloy is shown in Fig. 3. Fig. 4 is a depth profile from the same surface and indicates the thickness of the surface oxide to be about 120Å. The quantity of zinc within the oxide is low relative to the bulk level. The effect of exposure to the sodium borate solution is shown in Figs. 5-8. It is clear the thickness of the surface oxide increases from about to 120Å to about 3100Å upon 20 min exposure and to about 7000Å upon 60 min exposure. In addition, the concentration of zinc within the surface film increased with the exposure time. The observed zinc and magnesium oxide gradients in the surface film suggest that some of the magnesium oxide is leached out during

exposure to electrolyte solution resulting in zinc build up at the surface. The zinc concentration at the surface after 60 min exposure is estimated at about 70 wt% (18 at%). This enrichment of zinc at the surface explains why the long pre-exposure to the electrolyte results in greater passivity in the Mg-Zn alloys. The exact mechanism of passivation will be better understood after examination of all the data from both surfaces of the various Mg-Zn alloy ribbons, which is underway.

Surface analysis work on Mg-9.35 wt% Zn alloy in the as-rapidly solidified condition indicated the oxide on the free surface is slightly thinner (160Å versus 200Å) than on the wheel contact surface. This and the other binary alloys are being further examined to understand the role of the initial surface oxide on the film composition that develops upon exposure to the electrolyte and its effect on the corrosion rate.

5.2 Mg-Al Alloys: Detailed characterization and corrosion evaluations are being conducted on the Mg-14.4 wt% Al alloy. AES and XPS studies of the free and wheel contacts surfaces of this alloy in the as-rapidly solidified condition indicate very little compositional differences. A surface oxide deficient in aluminum was observed at the surface to a thickness of approximately 150Å. The effect various surface cleaning procedures such as glycol etch are being investigated to understand the role of oxides and cleaning procedures on surface chemistry and the corrosion behavior. Table III shows the XPS compositional estimates of the surfaces of this alloy.

5.3 Multicomponent Alloy 15: As mentioned earlier the complex alloy was selected to evaluate the role of various alloying elements of interest on the surface film formation due to rapid solidification and exposure to the electrolyte. As in the case of Mg-14.4 wt% Al alloy, this alloy exhibited only minor differences (see table III) in the surface chemistry among the two sides of the ribbon. The XPS depth-compositional profiles (Figs. 9 and 10) indicate the oxide thickness of the free surface is approximately 100Å, compared to about 150Å of the wheel contact surface. The oxide is primarily that of magnesium and little or no enrichment of lithium and aluminum are observed within the oxide. The chemical state plots of Mg, C and O (Figs. 11-13) obtained as function of depth indicate the presence of some of the surface carbon as carbonate and oxygen as hydroxide. Surface cleaning using glycol etch results in formation of a relatively thick (2900Å) oxide which contains little or no aluminum but contains traces of zinc and phosphorous (from glycol etch). These data are presented in Fig 14 and 15. Exposure of the ribbon (in the as-RS condition)to the electrolyte solution for 60 min results in the formation of a ~6300Å thick oxide. The XPS profile, shown in Fig. 16, also indicates that B, F, and Al are enriched within the top ~3000Å region, suggesting leaching out of magnesium from the near surface region.

leaching out of magnesium from the near surface region. All these results indicate dramatic changes that occur at the surface of a complex magnesium alloy as a result of simple chemical treatments and exposure to the electrolyte. Plans are underway to correlate this new information with the corrosion behavior of the treated alloy specimens.

6. SUMMARY

Selected Mg-Zn and Mg-Al binary alloys and a Mg-Al-Li-Zn-Mn-Ce multicomponent alloy were examined to understand their corrosion behavior in the as-rapidly solidified condition and upon selected surface chemical treatments. In addition surface characterization using AES and XPS was conducted to determine the role of surface chemistry on corrosion behavior. Surface films on both sides of the ribbons and their modifications due to chemical treatments including or exposure to sodium borate electrolyte were determined. Chemical treatments resulted in major changes in surface chemistry and surface film thickness which explain the differences in corrosion behavior. Experiments are continuing to fully understand these surface modifications and the precise mechanisms of corrosion. Some of the key observations are summarized below:

1. Most examined alloys, including the multicomponent alloy did not exhibit differences in EIS corrosion rates among the two sides of the ribbons. Mg-Zn alloys are the exceptions.

2. Surface oxides of most RS ribbons contain oxides of magnesium. Only lithium and calcium (among the alloys examined) have the tendency to be enriched in the oxide. The thickness and composition of the surface oxides vary with the bulk composition and with the cooling rate achieved during solidification. Carbonates and hydroxides were present at some of the examined surfaces and their role in corrosion needs to be understood.

3. Mg-Zn alloys exhibited differences in corrosion rates between the two sides of the RS ribbons, as function of the bulk composition and as function of the exposure time to the sodium borate electrolyte. Many of these differences can be explained by the surface chemical changes as determined by AES and XPS. Typically, longer exposure times and glycol etch cause formation of relatively thick films in the 2000-7000 Å range and with substantial enrichment of zinc near the surface region. In contrast, surface oxides of ribbons in the as-RS condition are deficient in zinc and are only 100-200 Å in thickness.

TABLE I. MAGNESIUM ALLOY COMPOSITIONS UNDER INVESTIGATION

Alloy	COMPOSITION in at% (wt% in parenthesis) Al	Li	Mn	Zn	Ce	Mg (BAL.)
Mg-14.4Al	13.2 (14.4)					86.8 (85.6)
Mg-28.8Al	26.7 (28.8)					73.3 (71.2)
Mg-42.8Al	40.3 (42.8)					59.7 (57.2)
Mg-4.8Zn				1.84 (4.8)		98.2 (95.2)
Mg-9.35Zn				3.7 (18.6)		96.3 (81.4)
Mg-18.6Zn				7.8 (18.6)		92.2 (81.4)
Mg-27.5Zn				12.4 (27.5)		87.6 (72.5)
15 (CAST)	5.95 (6.8)	11.56 (3.4)	0.18 (0.41)	0.93 (2.57)	0.60 (3.55)	80.79 (83.2)

TABLE II. CORROSION RESISTANCE OF RS Mg-Zn ALLOY RIBBONS DETERMINED BY EIS

Wt% Zinc	EXPOSURE TIME (min.)	CORROSION RATE (mpy)	
		Free Side	Wheel Side
0	20	53	46
	60	50	55
4.8	20	29	48
	60	125	118
9.35	20	56	98
	60	227	210
18.6	20	36	75
	60	152	161
27.5	20	15	61
	60	76	72

Corrosion rates were measured in 0.05 M sodium borate after exposure for 20 min or 60 min.

TABLE III. SUMMARY OF SURFACE COMPOSITIONS OF MAGNESIUM ALLOYS DETERMINED BY XPS

ALLOY	SURFACE*	CONDITION	SURFACE COMPOSITION (At.%)				
			Mg	Al	C	O	Other
Mg-14.4Al	FS	as RS	12.2	1.8	60.0	24.4	1.4 Si
		50Å Spu.	36.5	4.7	25.3	33.5	-
	WCS	as RS	11.4	1.7	67.0	18.6	1.3 Si
		50Å Spu.	33.5	4.7	31.4	28.3	2 Si
	WCS	etched**	3.3	1.9	71.1	22.7	1 Si
		etched + 50Å Spu.	8.6	4.7	62.9	23.9	-
Alloy 15	FS	as RS	6.3	1.4	31.0	40.0	21 Li
	WCS	as RS	6.5	0.8	33.0	42.0	17 Li
		as RS + expos. sod. Borate	12.2	4.0	24.5	47.9	8 B, 4 F, 0.1 Ce
		etched**	17.8	3.0	13.8	51.4	1 Zn, 13 P
		etched + expos. sod. Borate	47.0	5.3		42.3	5 B, 0.3 Ce

* Ribbon surfaces: FS - free surface
WCS - wheel contact surface

** Specimen was etched for 15 s using glycol etch.

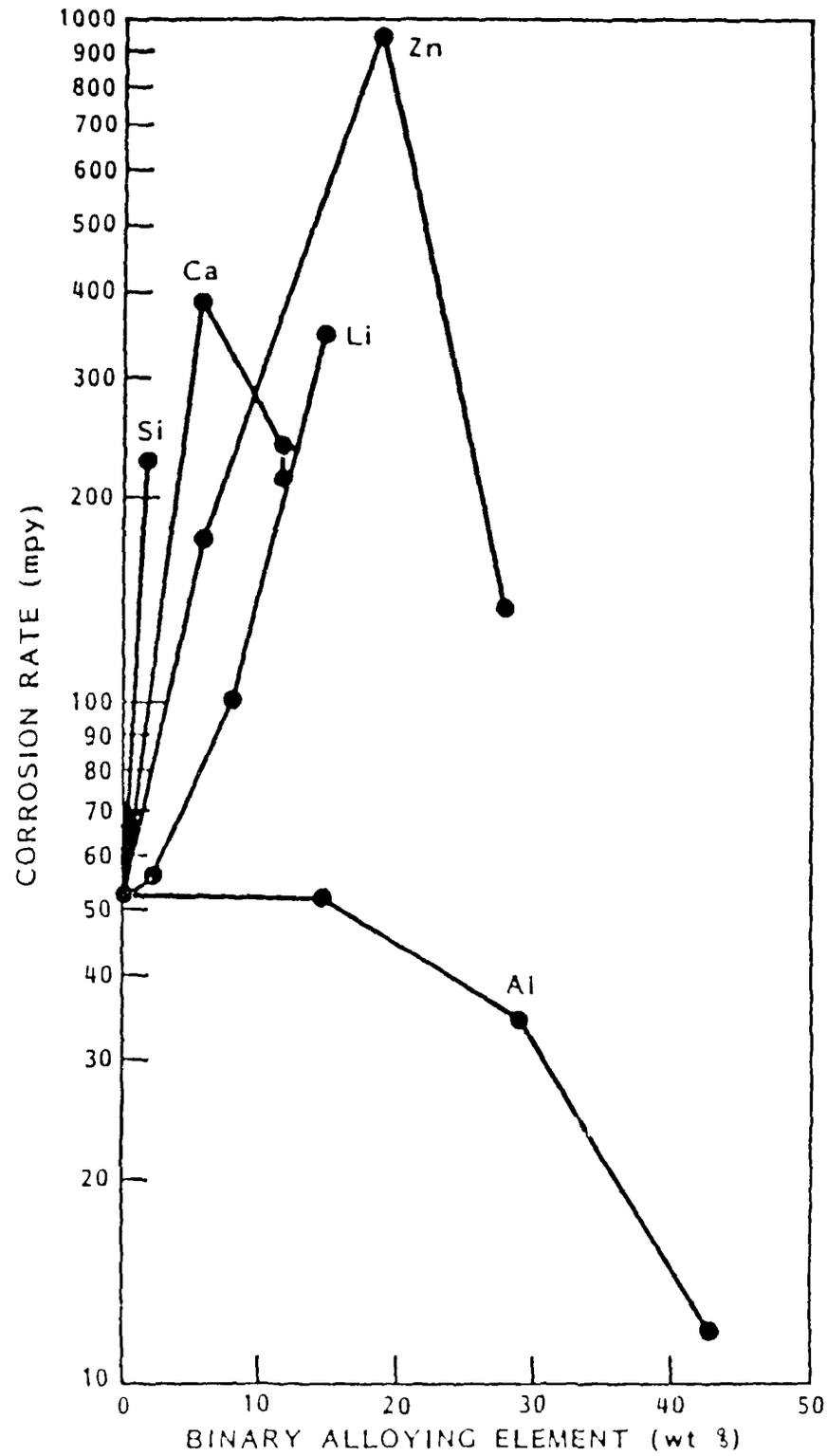

Fig.1. Corrosion rates of Magnesium binary alloys determined by EIS

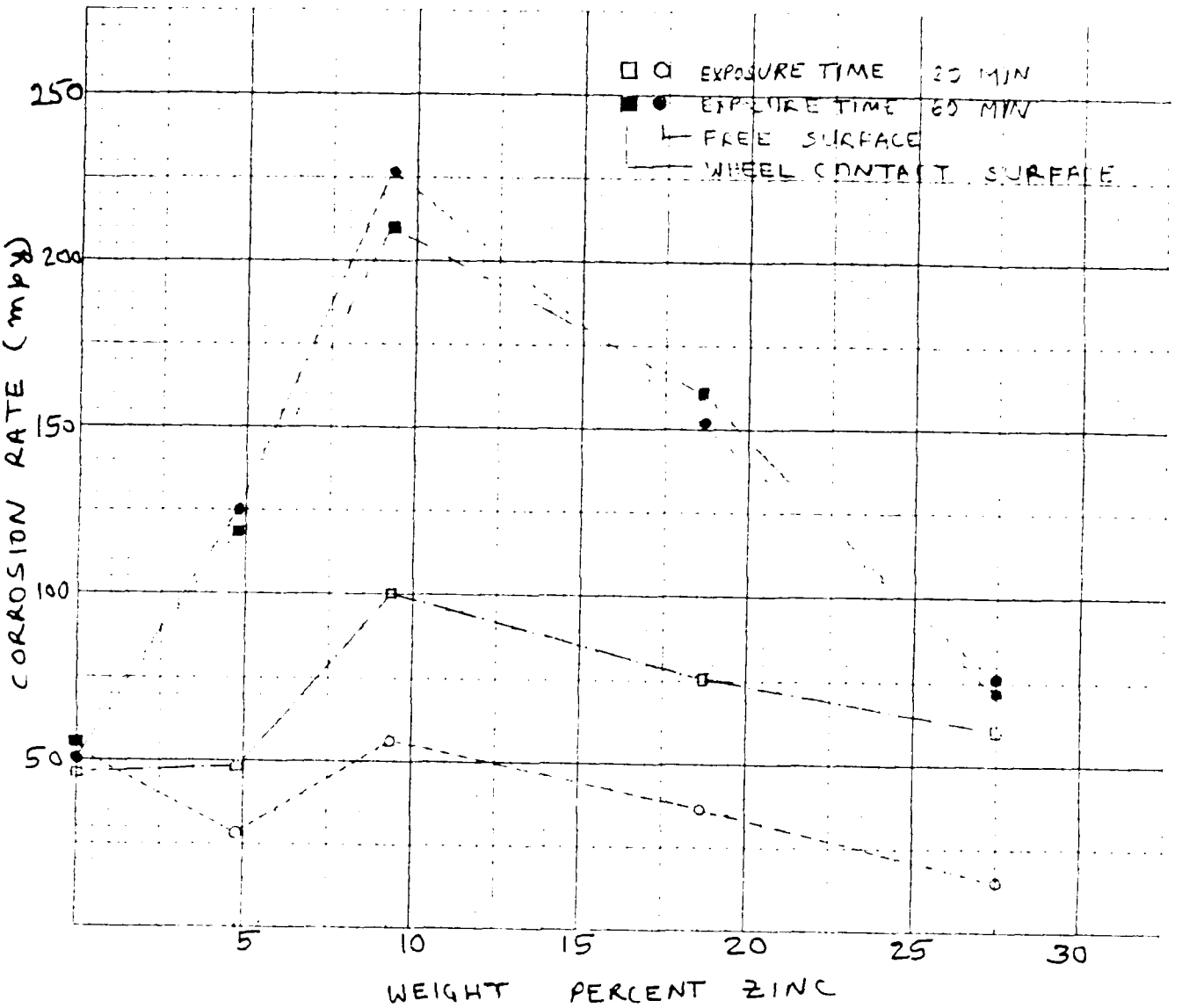

Fig.2. Corrosion rates of Mg-Zn binary alloys determined by EIS

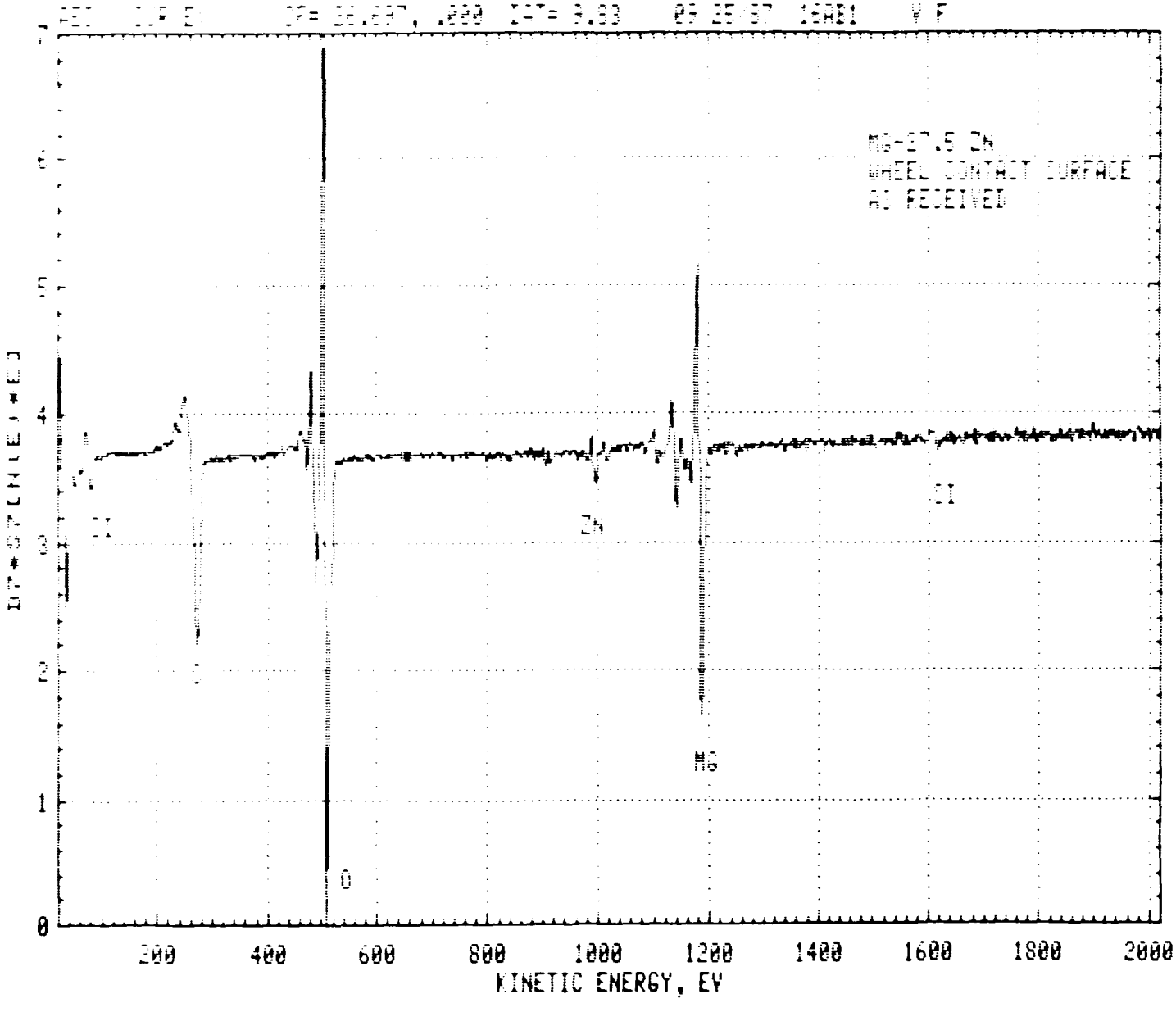

Fig.3. AES survey spectrum from the wheel contact surface of Mg-27.5 wt% Zn alloy

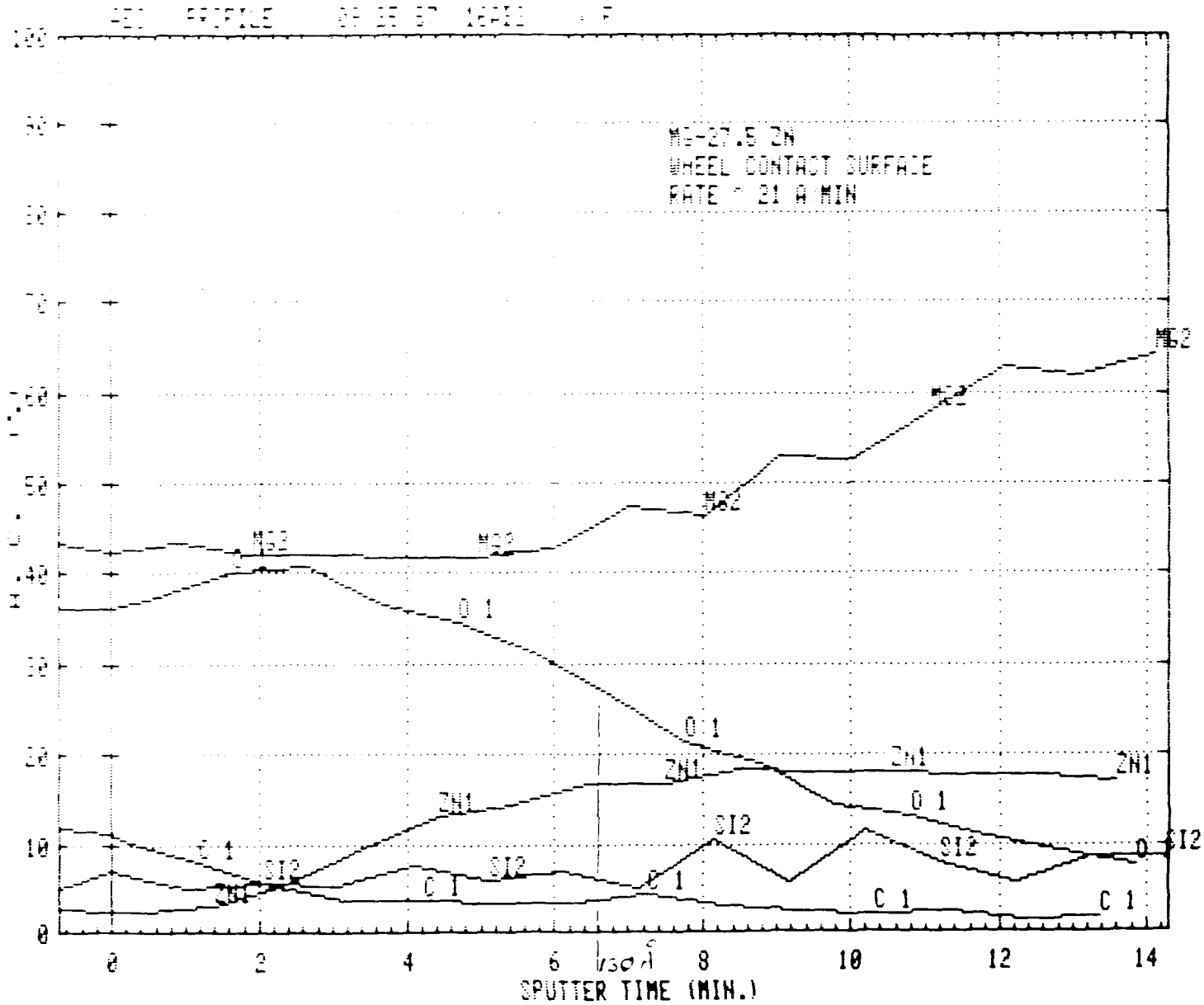

Fig.4. AES depth profile from the wheel contact surface of Mg-27.5 wt% Zn alloy

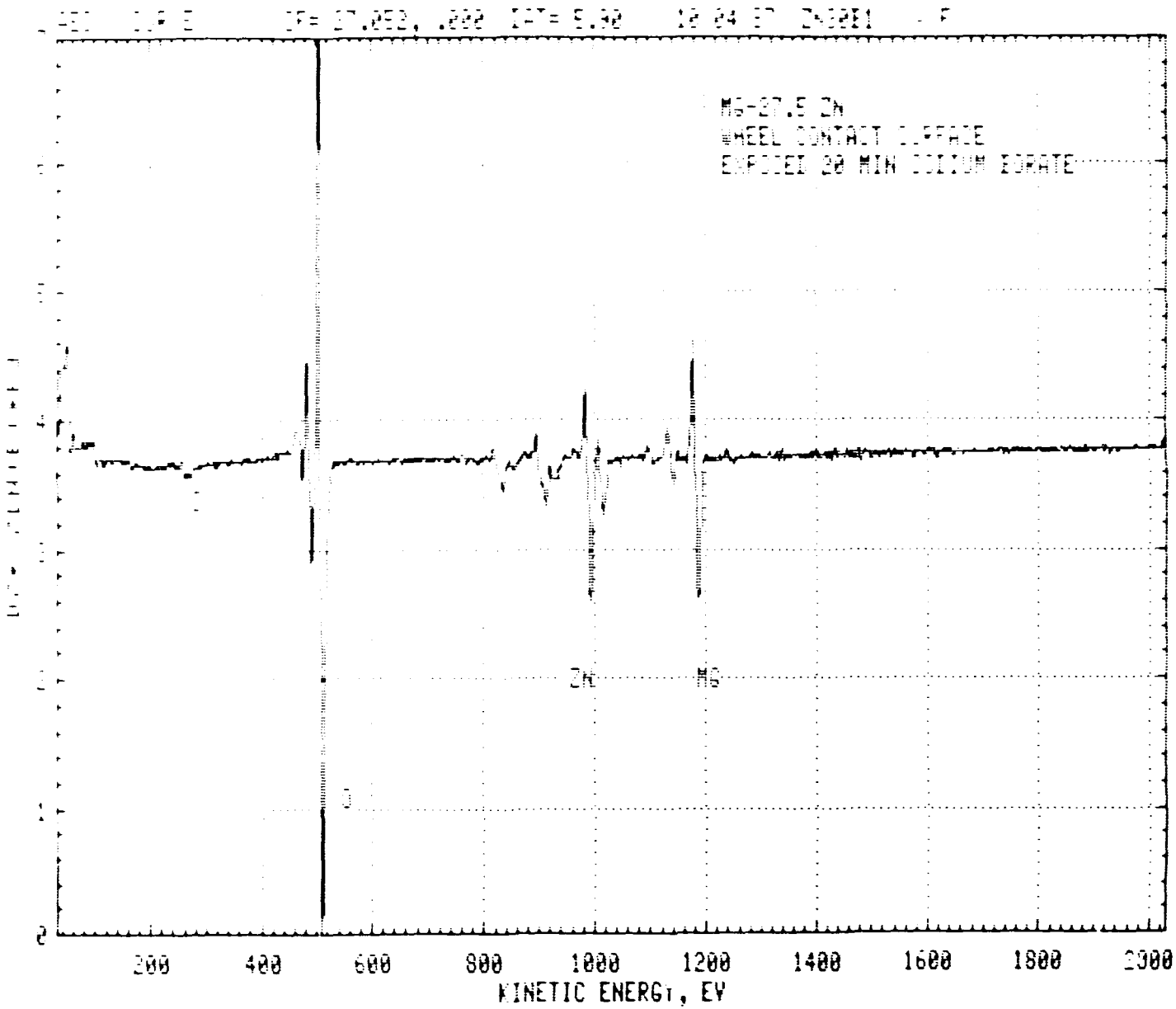

Fig.5. AES survey spectrum from the wheel contact surface of Mg-27.5 wt% Zn alloy, exposed 20 min to sodium borate

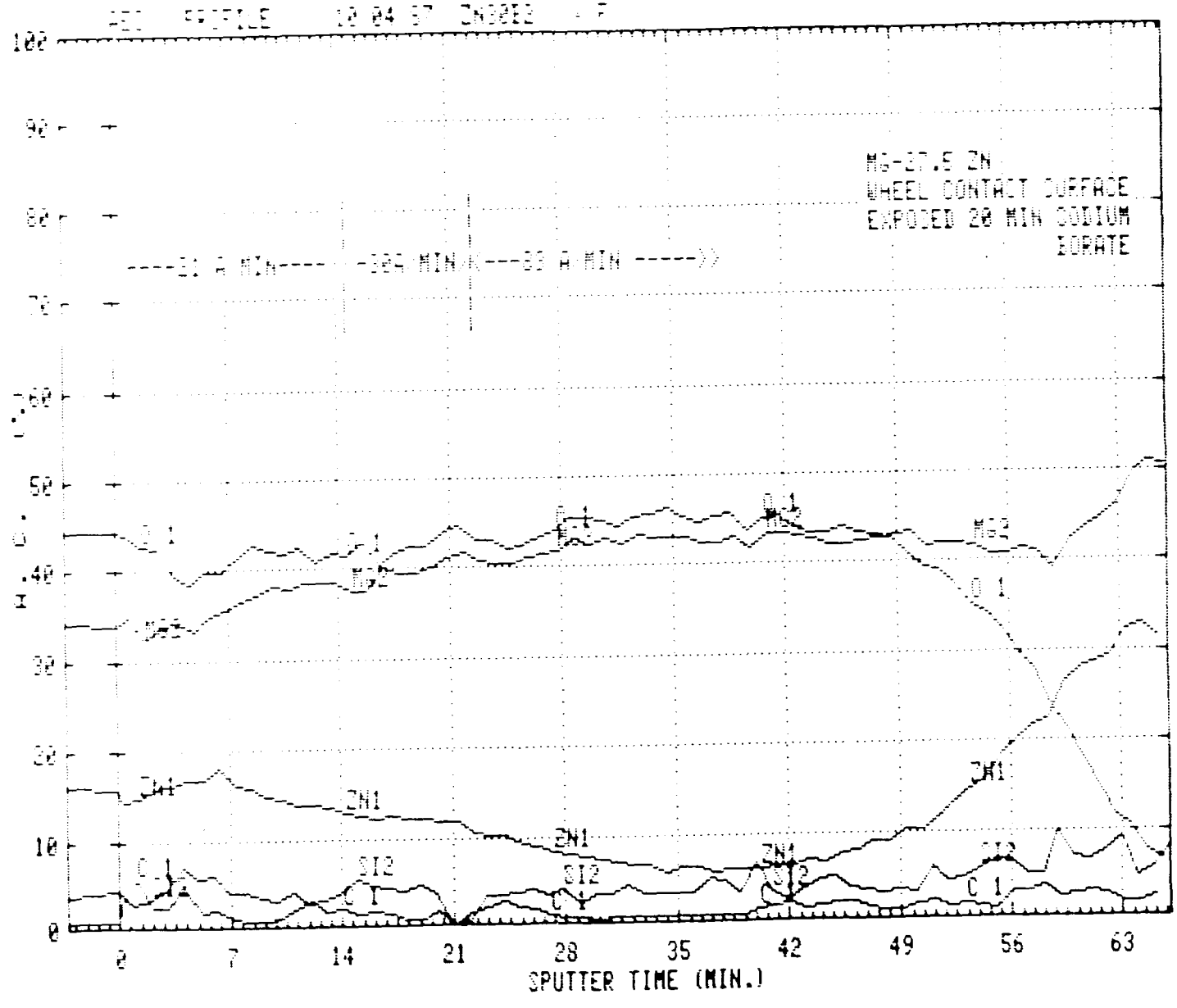

Fig.6. AES depth profile from the wheel contact surface of Mg-27.5 wt% Zn alloy, exposed 20 min to sodium borate

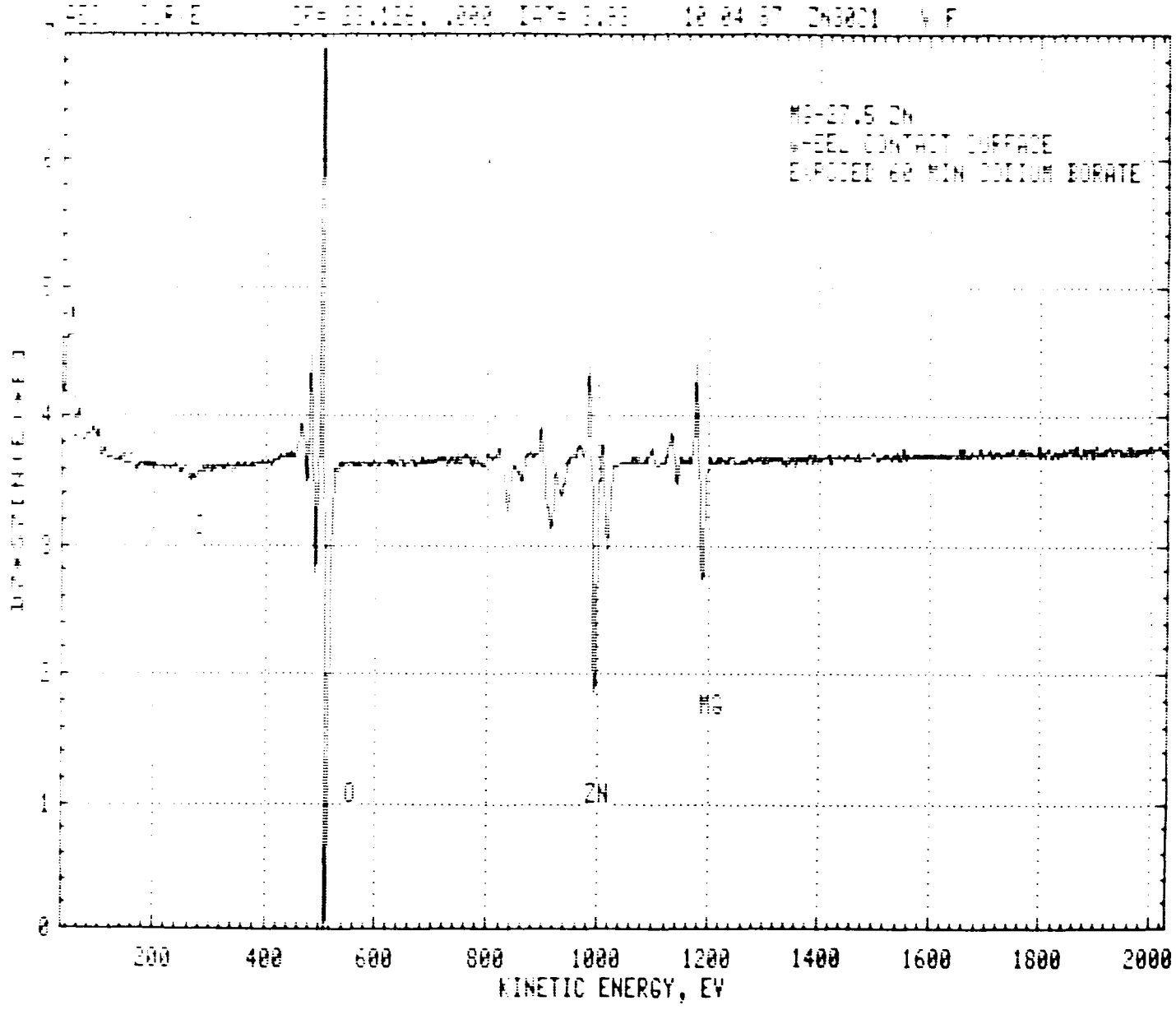

Fig.7. AES survey spectrum from the wheel contact surface of Mg-27.5 wt% Zn alloy, exposed 60 min to sodium borate

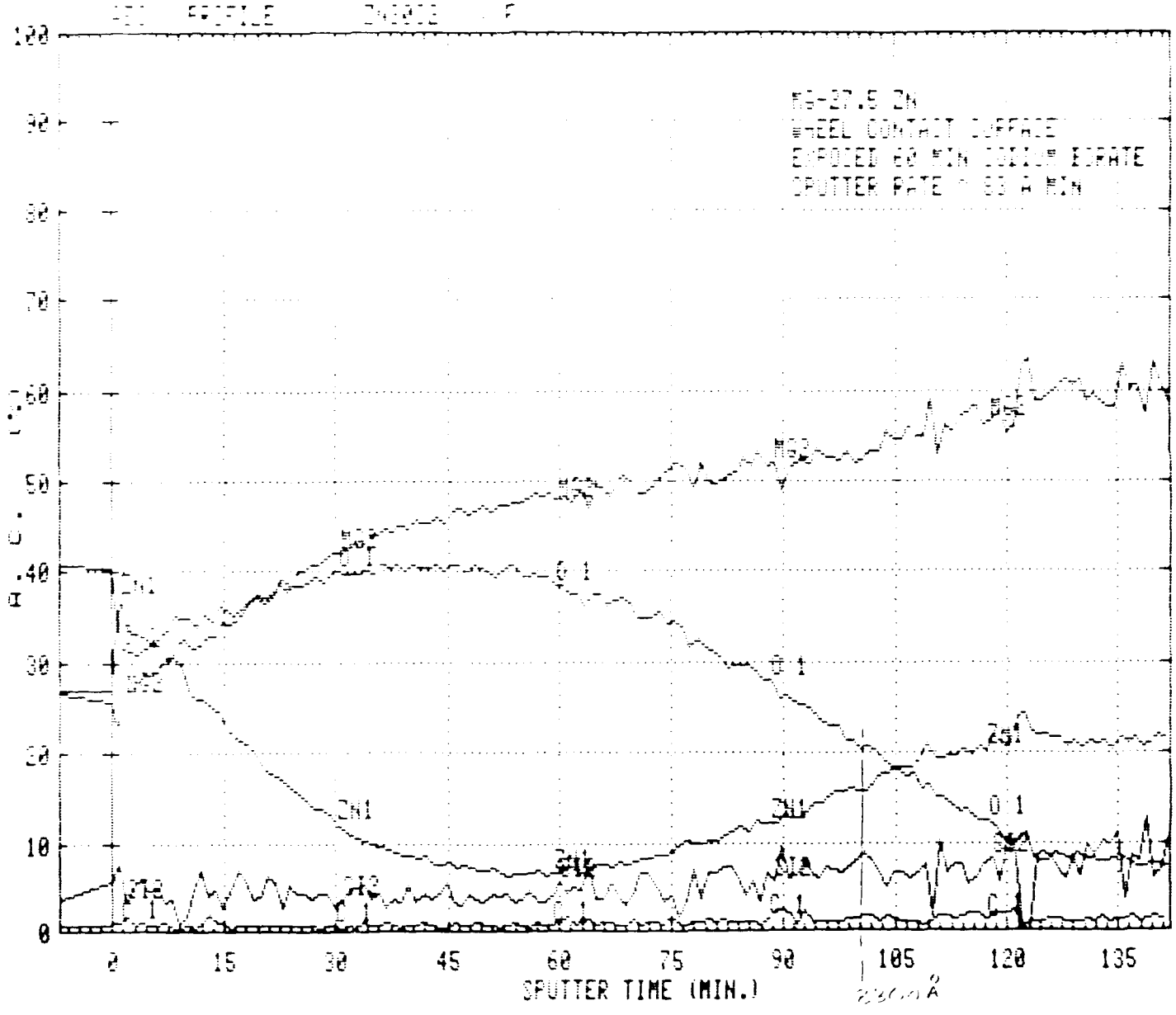

Fig.8. AES depth profile from the wheel contact surface of Mg-27.5 wt% Zn alloy, exposed 60 min to sodium borate

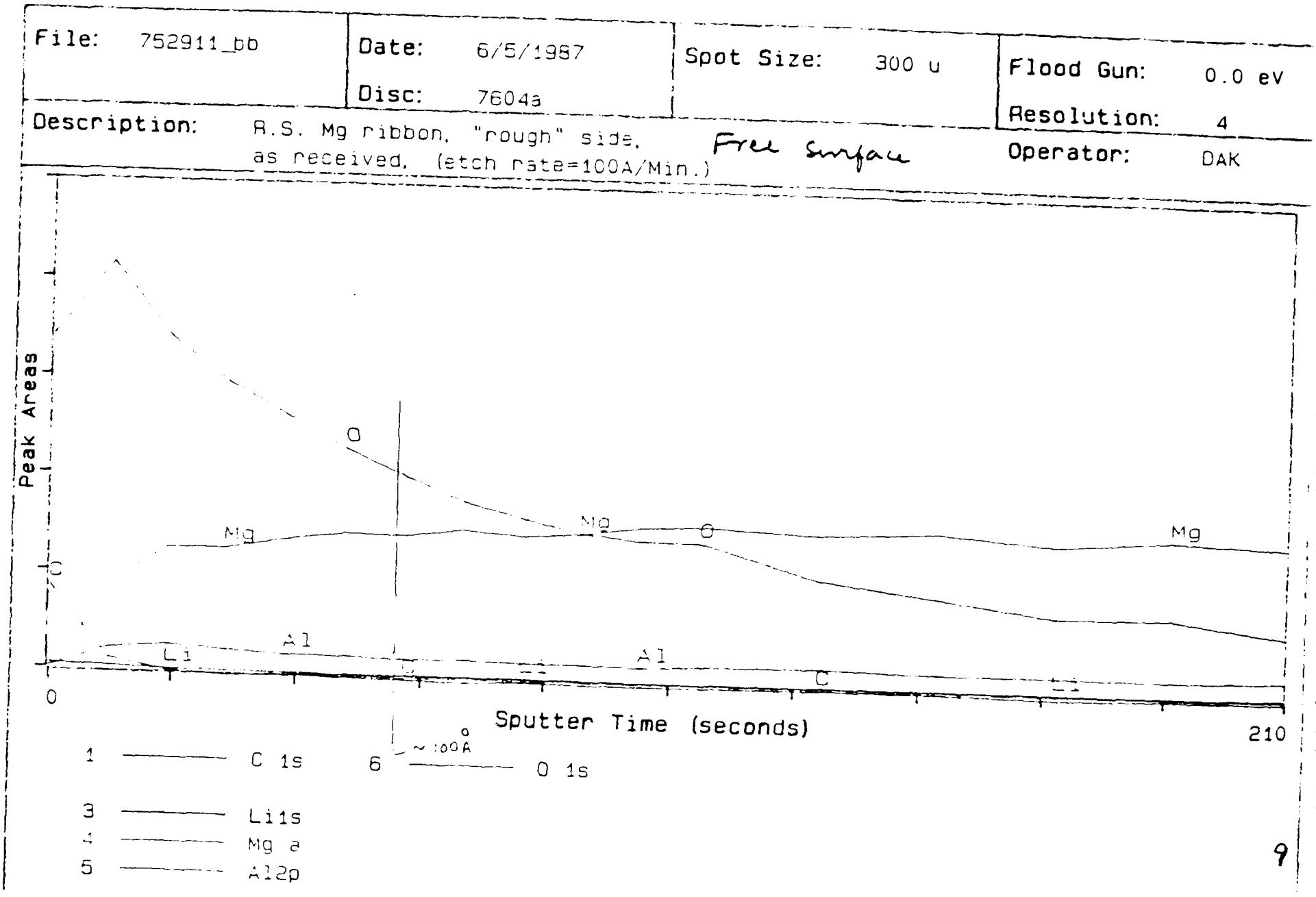

Fig.9. XPS depth profile from the free surface of alloy 15

File: 752911_cc	Date: 6/5/1987 Disc: 7605a	Spot Size: 300 u	Flood Gun: 0.0 eV Resolution: 4
Description: R.S. Mg ribbon, "smooth" side, as received. (etch rate=100A/Min.) wheel contact surface alloy #15 run #3			Operator: DAK

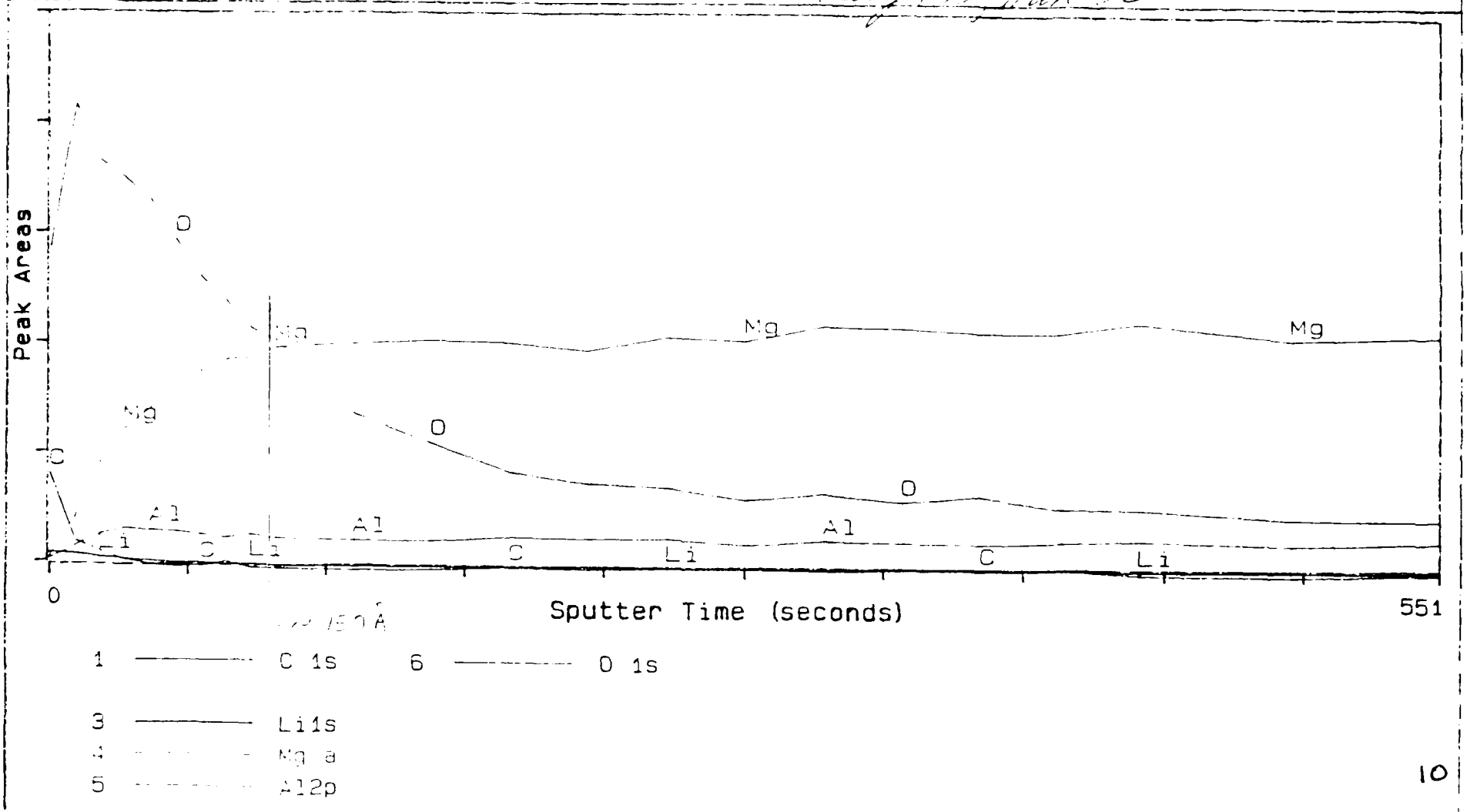

Fig.10. XPS depth profile from the wheel contact surface of alloy 15

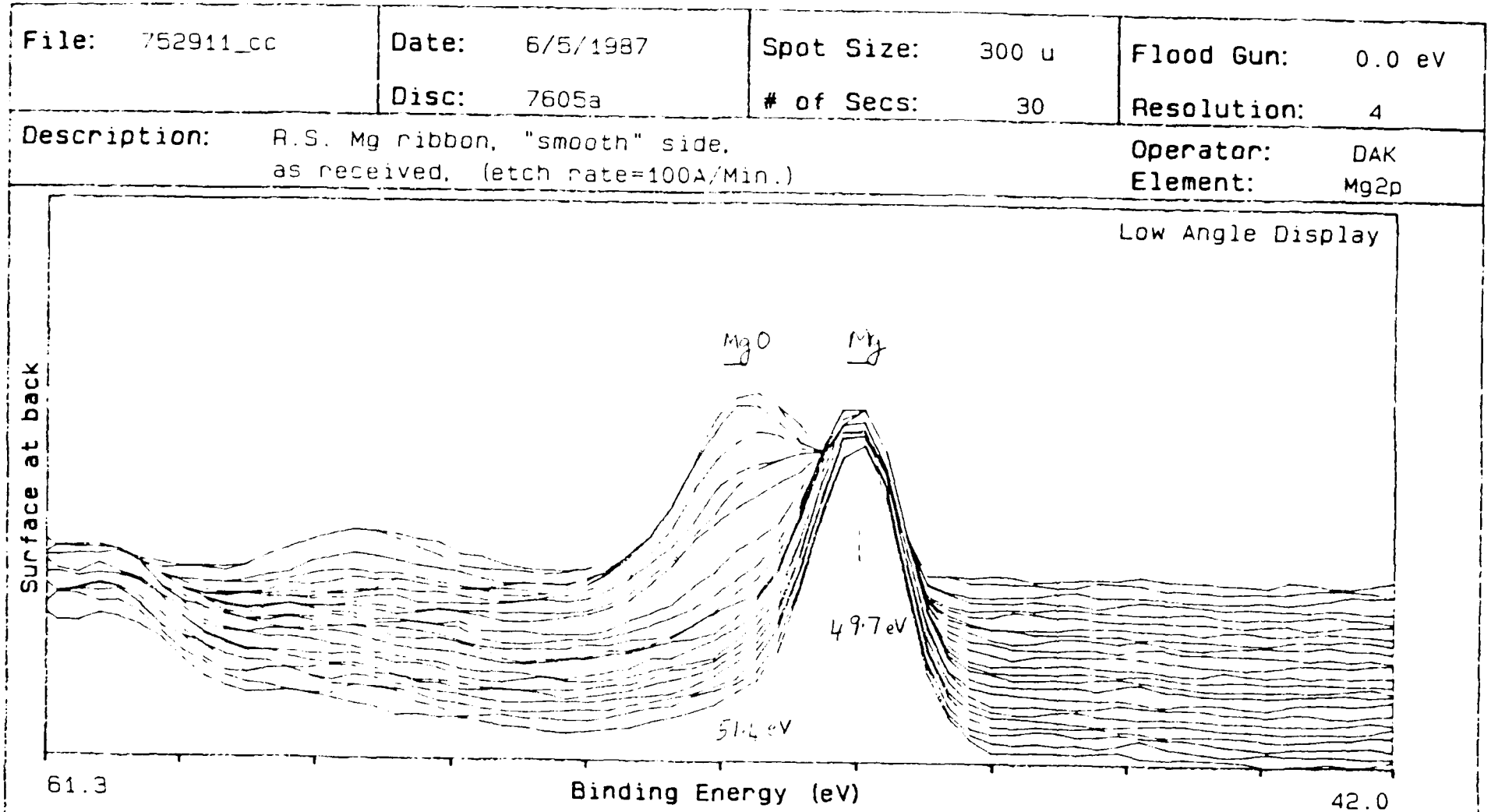

Fig.11. High resolution XPS spectra showing Mg_{2p} region as a function of depth from alloy 15, wheel contact surface

File: 752911_cc	Date: 6/5/1987	Spot Size: 300 u	Flood Gun: 0.0 eV
	Disc: 7605a	# of Secs: 10	Resolution: 4
Description: R.S. Mg ribbon, "smooth" side, as received, (etch rate=100A/Min.)			Operator: DAK Element: C 1s

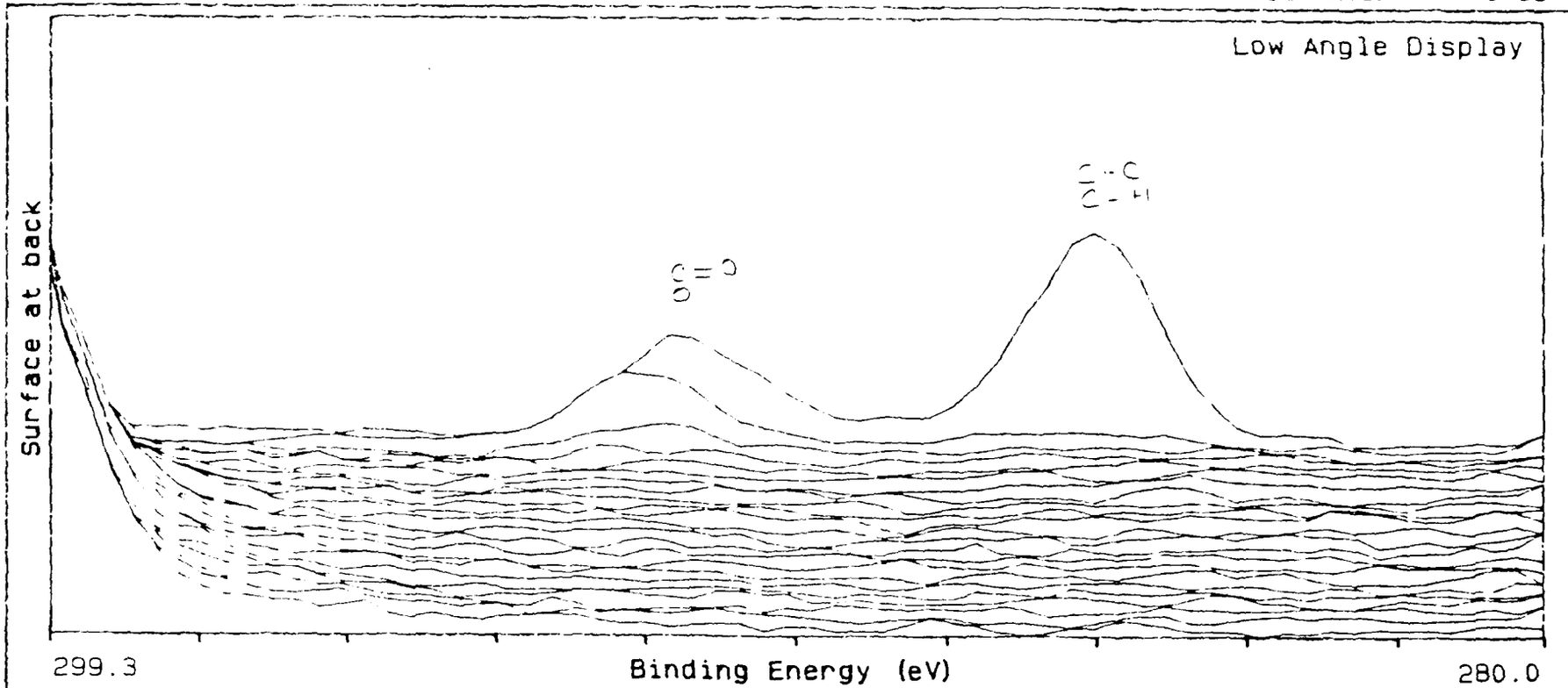

Fig.12. High resolution XPS spectra showing C_{1s} region as a function of depth from alloy 15, wheel contact surface

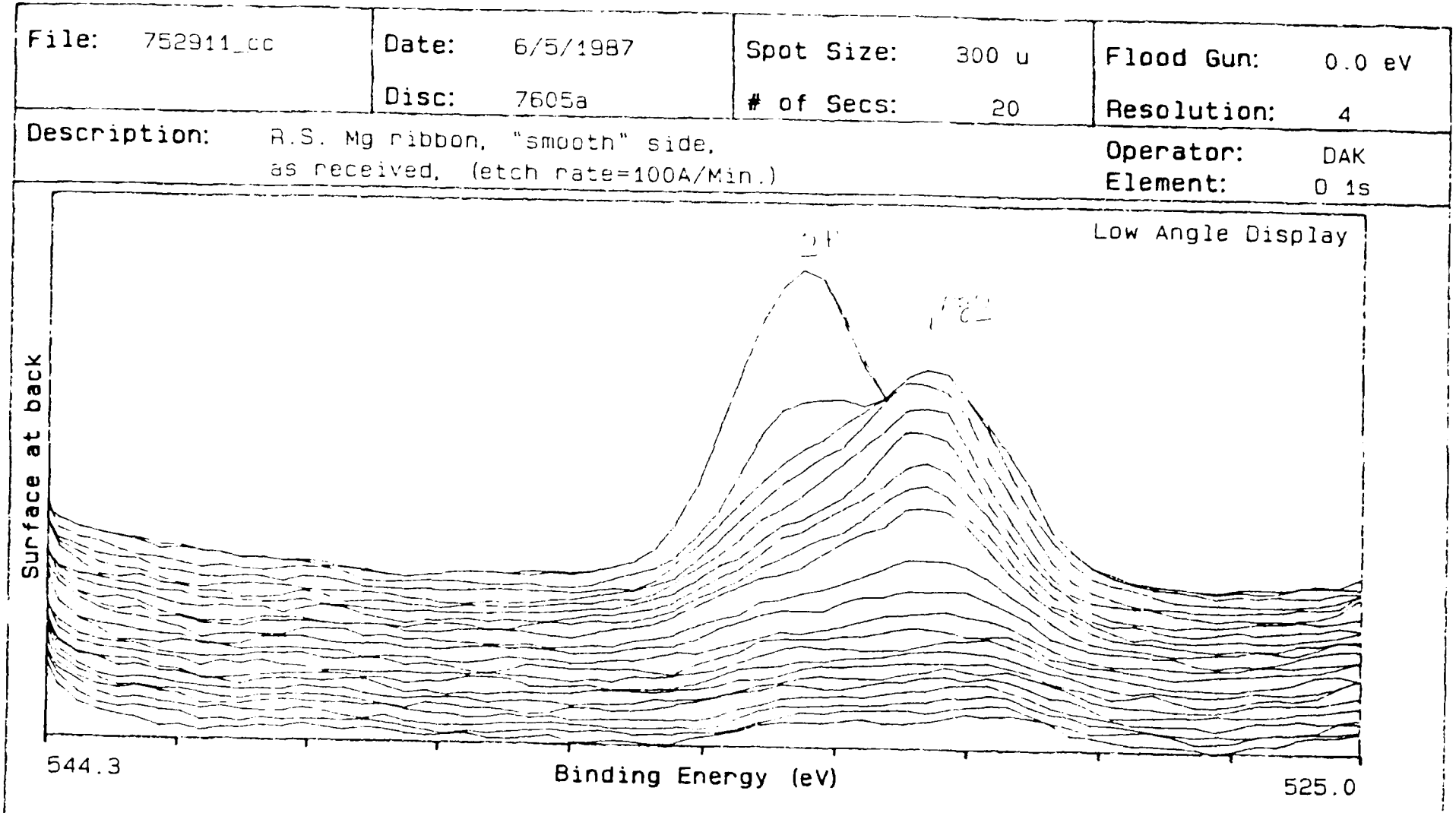

Fig.13. High resolution XPS spectra showing O_{1s} region as a function of depth from alloy 15, wheel contact surface

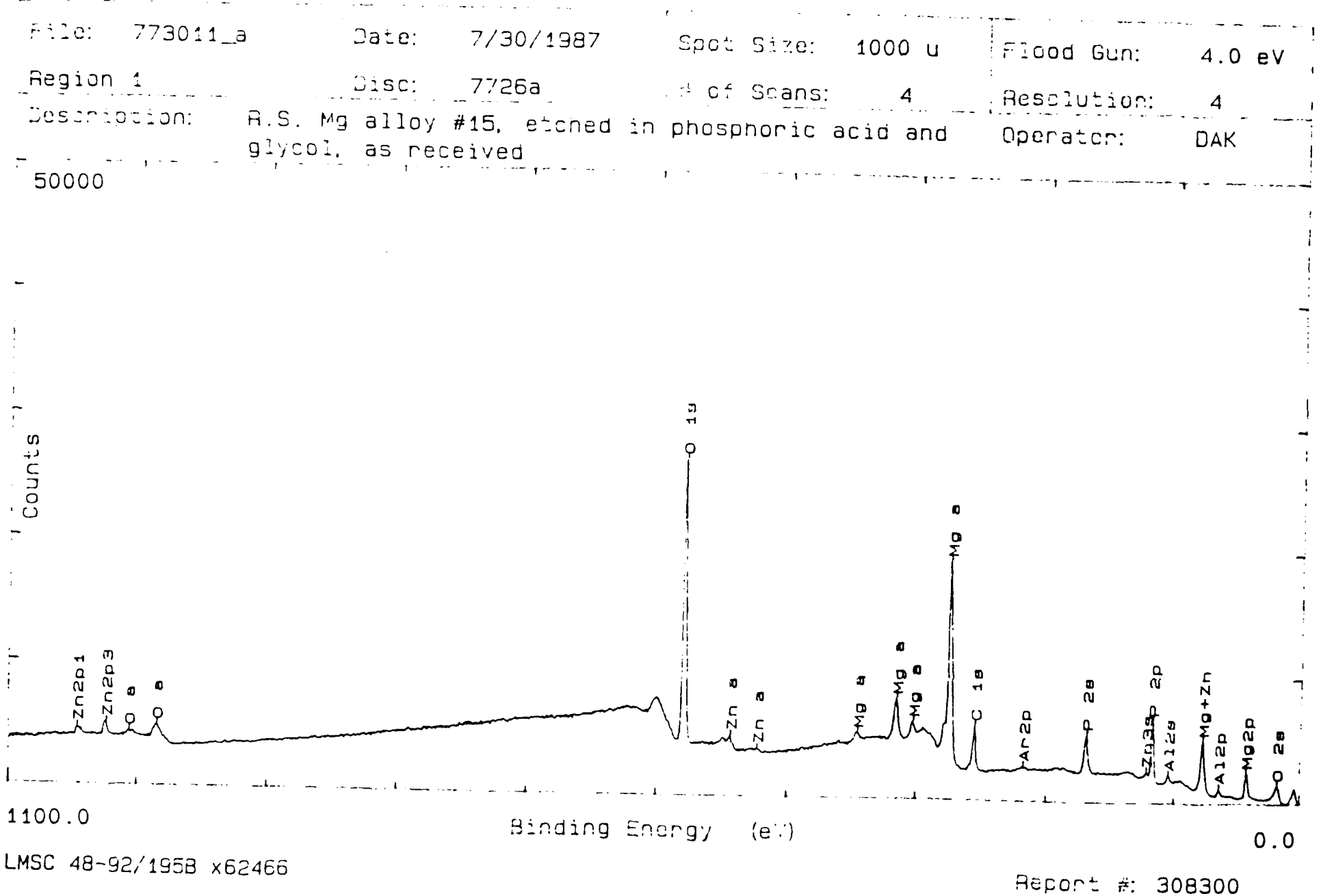

Fig.14. XPS survey spectrum of alloy 15, wheel contact surface in the etched condition

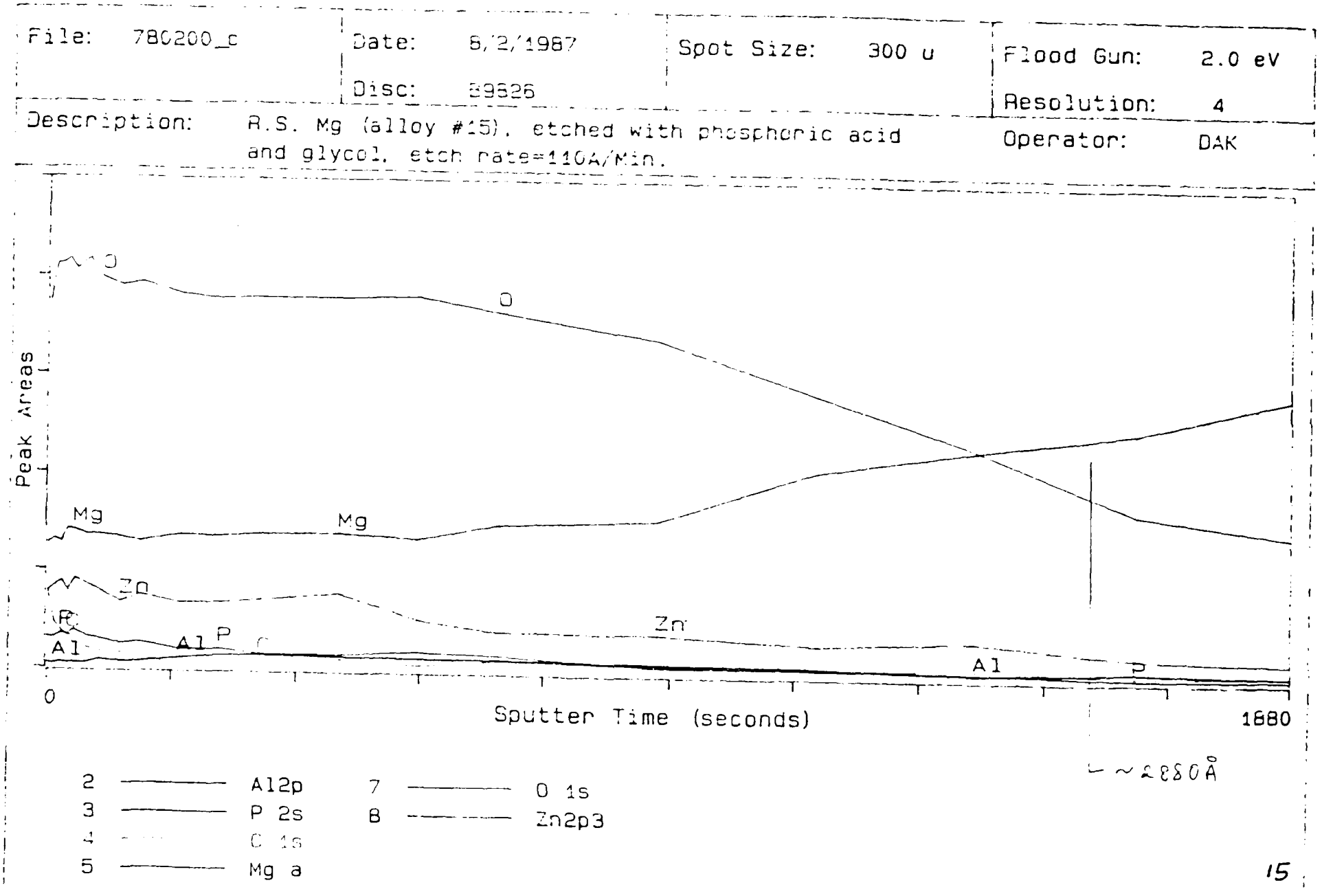

Fig.15. XPS depth profile of alloy 15, wheel contact surface in the etched condition

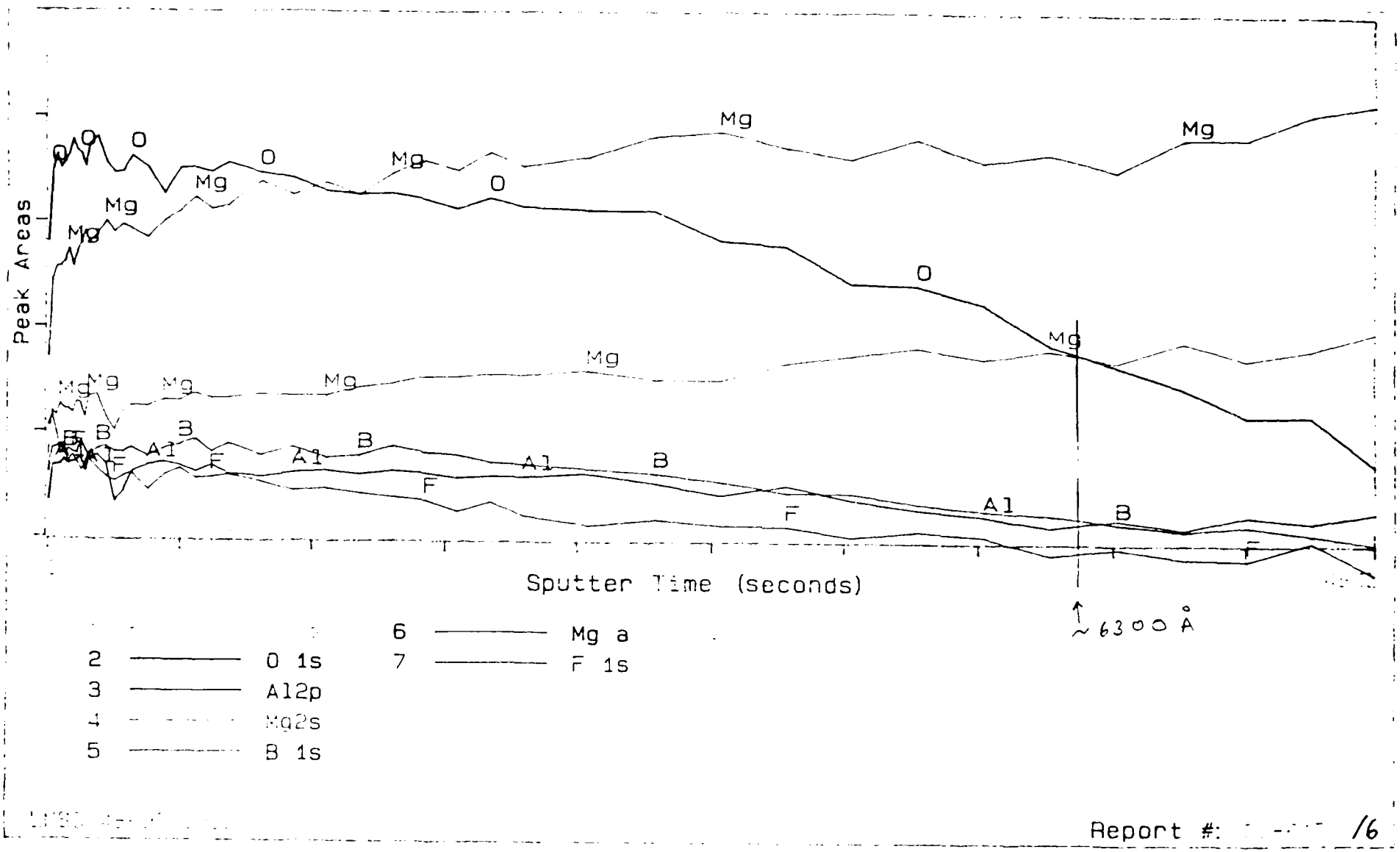

Fig.16. XPS depth profile of alloy 15, wheel contact surface after exposure to sodium borate solution for 60 min

PUBLICATIONS

1. ReflEXAFS of Thin Films on Mg and Mg Alloys, G.G. Long, D.R. Black, G.A. Danko, D.K. Tanaka, Z. Zhang and J. Kruger, Annual Report NSLS 1987, in press.

2. Structure of Surface Films on Mg and Mg Alloys, G.G. Long, J. Kruger, D.K. Tanaka, and Z. Zhang, to be submitted to J. Electrochem. Soc.

3. Surface X-Ray Absorption Spectroscopy, EXAFS and NEXAFS, for the In Situ and Ex Situ Study of Electrodes, Chapter in Techniques for Characterization of Electrodes and Electrochemical Processes, John Wiley & Sons, in press.

4. Corrosion of RSP Mg Alloys, G.L. Makar and J. Kruger, to be submitted to Corrosion.

END

DATE

3-88

DTIC